3DMedNet

Top articles of 2017

TOP ARTICLES SUPPLEMENT

CONTENTS

fsg CONNECT

Short Communication

For reprint orders, please contact: reprints@futuremedicine.com

Journal of
3D Printing in Medicine

In situ functionalization of scaffolds during extrusion-based 3D plotting using a piezoelectric nanoliter pipette

Stefan Giron[1], Anja Lode[1] & Michael Gelinsky*[,1]

[1]Centre for Translational Bone, Joint & Soft Tissue Research, University Hospital Carl Gustav Carus & Faculty of Medicine, Technische Universität Dresden, Fetscherstr. 74, 01307 Dresden, Germany

*Author for correspondence: michael.gelinsky@tu-dresden.de

Additive manufacturing techniques can be applied to individually craft medical implants and biomaterial scaffolds. We present the combination of macroscopic scaffold fabrication by strand deposition and high-resolution dosing of liquids using the 'BioScaffolder 2.1' 3D plotter from GeSiM with an integrated piezoelectric nanoliter pipette. A fluorescein solution, used as model substance, was dispensed on calcium phosphate bone cement strands during scaffold production; high reproducibility of the alternating subprocesses was demonstrated. Moreover, the release kinetics of VEGF loaded onto flat calcium phosphate cement substrates was investigated. The presented approach opens up new and exciting possibilities for tissue engineering. Various biological components can be integrated precisely into 3D scaffolds according to a predefined pattern creating tissue equivalents of high complexity.

First draft submitted: 7 June 2016; Accepted for publication: 30 August 2016; Published online: 13 October 2016

Keywords: 3D printers • drug delivery • technology

In recent years, additive manufacturing techniques have become a promising approach in regenerative medicine. Especially, 3D printing with modified inkjet printers has allowed creating well-designed living constructs thanks to the high-resolution positioning of small droplets of bioink and ease of use [1]. However, this method is restricted by the low viscosity of suitable bioinks, resulting in rather flat geometries [1,2]. In contrast, extrusion-based 3D printing or 3D plotting offers the opportunity to process a broad range of different pasty materials with high viscosities under mild conditions [3–5]. Therefore, fabrication of scaffolds with dimensions of several centimeters is possible. The mild process conditions basically allow the integration of biological factors. However, this might require complex additional steps for loading [6,7] and drastically reduces the number of suitable materials – the latter, especially if cells should be incorporated. In this work, the 3D plotting technique was expanded by adding a piezoelectric dispensing device with the aim to functionalize the 3D scaffolds during their manufacturing.

Although the plotting process results in macroscopic constructs, they may be easily modified with solutions of various different substances on a submillimeter scale. Thus, local patterning with drugs or active substances like growth factors to guide cell adhesion or cell fate using printing technologies previously mostly limited to 2D substrates now becomes possible during fabrication of 3D scaffolds. Besides this alternative loading method without the need to mix the biological component into the plotting paste and thereby defining its concentration, this approach also facilitates the localized deposition of different cell types.

In this study, we have chosen a pasty, self-setting calcium phosphate bone cement (CPC) as plotting material and an aqueous fluorescein solution as model substance for local modification during scaffold

Future Medicine part of fsg

fabrication. Additionally, a release experiment with VEGF was conducted to test whether the method of application possibly interferes with the agent in use. Recently, we have shown homogeneous functionalization of the same type of CPC with VEGF by mixing of both components prior to manufacturing of 3D scaffolds for bone tissue engineering by 3D plotting [7].

Materials & methods

Scaffold fabrication by 3D plotting

3D plotting was carried out using a commercially available BioScaffolder 2.1 from GeSiM (Radeberg, Germany) with an integrated 'Nano Tip' piezoelectric pipetting unit. An α-tricalcium phosphate-based hydroxyapatite forming CPC (Velox™ from InnoTERE, Radebeul, Germany) was used as plotting paste in which the solid precursor mixture is suspended in an oily liquid [4,8]. The paste was extruded from a cartridge (NordsonEFD, Dunstable, UK) via a dosing needle with an inner diameter of 610 µm (Globaco, Roedermark, Germany) using compressed air at a pressure of 250 kPa and a speed of 9.7 mm/s. The strands were deposited layer by layer according to a predefined layout realizing the 3D scaffold. To cut off the strands at the end, a horizontal tear off of 3 mm was implemented with a tear-off speed of 30 mm/s.

Integration of piezoelectric pipetting into the 3D plotting process

A 0.1 mM fluorescein solution that had been prepared from fluorescein diacetate (Sigma-Aldrich, Taufkirchen, Germany) according to McKinney *et al.* [9] was used as a model liquid to test the ability to combine 3D plotting and pipetting. The solution was picked up from a 96-well tissue culture polystyrene (TCPS) plate (Greiner Bio-One, Frickenhausen, Germany) directly before pipetting using the piezoelectric pipetting unit with a so-called 'Nano Tip' (GeSiM). An integrated stroboscope was used to check the dispensing behavior. Theoretically, the size of dispensed drops may be adjusted by changing the pulse length and voltage applied to the pipette's piezo actor. In practice, these parameters were used to adjust the fluid properties of the dispensed liquids and minor differences of the pipette in use in order to guarantee reproducible dispensing of drops consisting of about 0.5 nl each. The applied voltage was 70 V at a frequency of 100 Hz and a width of 60 µs for the rectangular pulse. To increase the dispensed volume, several drops were put on the same position.

The movement of both the devices, the plotting cartridge and the piezopipette, was controlled by the three-axis motion system of the BioScaffolder. The actual pipetting was carried out when the pipette was at rest. First, a layer of three parallel CPC strands was plotted. Second, fluorescein solution was pipetted on top of these strands. Third, a second layer of CPC was put onto the strands of the first layer creating perpendicular crossings. Fourth, fluorescein was pipetted on the strands of the second layer and so forth until eight layers of CPC were deposited in total. The intended layout is sketched in Figure 1A.

Light microscopy

Images were recorded with a Leica M205C stereomicroscope (Leica Microsystems, Wetzlar, Germany). The GNU Image Manipulation Program (GIMP, version 2.8.10) [10] was used for image processing.

Release experiment

In order to check whether the pipetting alters the release kinetics, recombinant human VEGF-A_{165} (Biomol, Hamburg, Germany) was pipetted on preset CPC samples. A concentration of 100 µg/ml was used with the 'Nano Tip' and 10 µg/ml with conventional pipettes ('Research,' Eppendorf, Hamburg, Germany). The samples were prepared from the same CPC paste used for 3D plotting. Those flat disks with 10-mm diameter and 1-mm height were produced with a silicone mold and had been set in water-saturated atmosphere at 37°C for 3 days [7]. Afterward, the CPC disks have been washed twice, disinfected by immersion in 70% ethanol for 15 min and rinsed again with 70% ethanol before air drying. All samples were placed in 48-well TCPS plates (Nalge Nunc International, Roskilde, Denmark), which had been incubated with 1% bovine serum albumin (Sigma-Aldrich) in phosphate-buffered saline (Gibco Life Technologies, CA, USA) overnight in order to prevent binding of VEGF to the plastic surface. The VEGF solution was prepared in a 96-well TCPS plate (Greiner) that was also incubated overnight with 1% bovine serum albumin in phosphate-buffered saline. Four samples were loaded with 46-ng VEGF each by dispensing a simple pattern of 1000 drops of about 0.46 nl with the piezoelectric pipette. Three controls with 50 ng have been prepared using manual pipetting and one CPC disk without VEGF was used as negative control. The release was started 30 min after the pipetting using α-minimum essential medium (MEM; BioChrom, Berlin, Germany) with 9% fetal calf serum as the release medium. After 2 h and afterward every 24 h, the release medium has been replaced for a total release interval of 7 days. The amount of released VEGF was determined by an ELISA following standard protocols described previously [11].

Although the release experiment was carried out under cell-culture conditions, the pipetting itself was not strictly sterile in the current setup of the

BioScaffolder. Though operated in a sterile workbench, the pipetting unit could only be disinfected by rinsing the pipette and the tubes of the hydraulic system with 70% ethanol for several minutes. Automatic cleaning procedures used the so-called 'system water' that was in contact with the pipette and the tubes, breaking sterility. Nonetheless, no contamination has occurred, neither in the release experiment, nor in experiments with living cells not described here.

Results & discussion

It could be demonstrated in previous studies [4,7] that the CPC, used here as biomaterial for scaffold fabrication, is a suitable pasty material for extrusion-based 3D plotting. As it is a self-setting material, no other treatment than immersion in aqueous media or contact with humidity is required to form mechanically stable constructs. By varying needle diameter and strand distance as well as strand orientation in neighboring layers, a variety of geometries can easily be realized [4,7,12].

We now have been able to dispense very small volumes of a liquid onto plotted scaffolds *in situ* during the computer-aided manufacturing process under mild conditions. The scaffolds consisting of eight CPC layers, shown in Figure 1, have been realized by alternating 3D plotting and piezopipetting. The plotted strands have been used as the spatial reference for the pipetting process. After calibration, the fluorescein solution could be placed on top of the strands with high accuracy. By varying the number of drops dispensed at each position from 1 to 32, a fluorescein gradient was created. The application of different liquids even in one layer is also feasible; however, it is not shown. As a washing step is necessary when changing the liquid, the remaining volume is wasted and the overall production time is increased. Thus, the number of liquid changes should be minimized by design. Smaller volumes per droplet could be achieved using a 'Pico Tip,' also available as a tool for the GeSiM BioScaffolders.

The presented combination of 3D plotting and pipetting enables us to create scaffolds with complex patterns of functional substances. Though the resolution of the pipetting was shown to be generally excellent, the liquid/material combination always has to be taken into account, especially when fast diffusion of the liquid on or into the underlying strand might occur. The use of hydrogels in former studies [5,13,14] already showed that cells may be directly incorporated into scaffolds with clinically relevant dimensions. With integrated pipetting, the range of scaffold materials that may be seeded with live cells during 3D fabrication can be widened as the cells are not to be immersed in the plotting pastes. Immiscible fluids may also be locally dispensed, as shown with

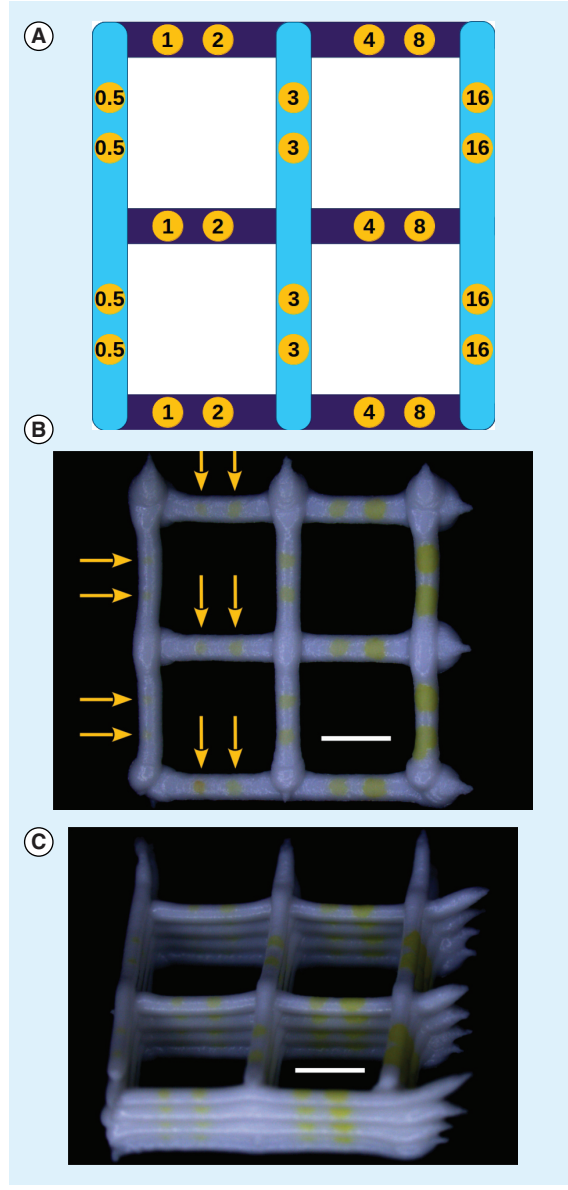

Figure 1. Functionalization of a plotted 3D scaffold during manufacturing with small volumes of a liquid solution. (A) Scheme of the scaffolds shown in parts **(B)** and **(C)** indicating the pipetted volume at each position in nanoliters. The two different colors of the strands represent the two layers, printed on top of each other. **(B)** Light microscopic image of a plotted CPC scaffold with approximately 0.7 mm strand diameter and pipetted spots with 0.1 mM fluorescein solution, visible by its bright yellow color. Arrows point at small spots. The lateral resolution depends highly on the dispensed volume. **(C)** Light microscopic image of a 3D scaffold with eight layers realizing the scheme **(A)** four-times. Note that the fluorescein spots are partially covered by the strands of the following layer. Depending on the pasty material and the chosen geometry, this is not necessarily the case. The resolution in the direction perpendicular to the layers is additionally limited by the strand height. Scale bars correspond to 2 mm. CPC: Calcium phosphate cement.

the water-based fluorescein solution on the oil containing hydrophobic CPC strands. Furthermore, the pipetting allows tailoring of the local concentrations of drugs or biological factors (or the cell seeding density) unlike the homogeneous distribution provided by mixing the plotting paste with the substance or cells, respectively. The pasty materials utilized for 3D plotting are restricted to those that may be processed without buoyancy compensation, in other words, extrusion into a liquid plotting medium [15]. In contrast to inkjet printing and 3D plotting, where the number of different liquids and their combinations is limited by the number of available cartridges, the pipetting enables the local integration of many different substances or even different cell types into one single scaffold. This is possible since the liquids are picked up from 96-well plates during scaffold synthesis. The applicability of the piezoelectric nanoliter pipette for cell positioning was already proven. Jonczyk *et al.* have shown very recently localized cell seeding of the human lung carcinoma cell line A-549 used as model in 2D with a 'NanoPlotter' (GeSiM), utilizing the same pipetting unit [16]. Moreover, we were also able to locally seed cells of an osteosarcoma cell line (SAOS-2) into TCPS well plates as well as on collagen membranes with the BioScaffolder (data not shown).

The VEGF solution, automatically pipetted onto a flat CPC substrate, showed the same release kinetics as the manually pipetted growth factor. The data from ELISA are displayed in Figure 2. In both cases, a large initial burst was observed, releasing approximately 93% of the VEGF within the first 2 h. After 24 h, the release was basically complete. In contrast, a slow and only partial release was observed when VEGF (adhered to chitosan microparticles) was mixed homogeneously with the CPC paste prior to scaffold fabrication by 3D plotting. In this study, preservation of biological activity of the released growth factor was verified in direct and indirect cell culture experiments [7]; therefore, it is very likely that VEGF dosing by piezopipetting does not alter bioactivity as it is a much less invasive process compared with direct inclusion in the plotting paste.

The very quick VEGF release in the present study was due to the short time period of 30 min from loading to release. Lode *et al.* showed in a similar setup that the release would be delayed by longer loading periods [17]. Also a modification by adding heparin to the CPC was shown to result in a slower release with reduced initial burst [17]. Furthermore, the release kinetics might be altered independently from the specific biological factor by enclosing it between strands, either on crossings or in full length, when multiple strands are plotted onto another in the same orientation. Owing to the fact that the liquids can only be dispensed onto the top of the strands, the high resolution of scaffold functionalization can only be achieved on the level of each single layer; perpendicular to the layers, the resolution is limited by the strand diameter. In practice, the resolution depends highly on the dispensed volume and the wetting of the liquid/paste material combination.

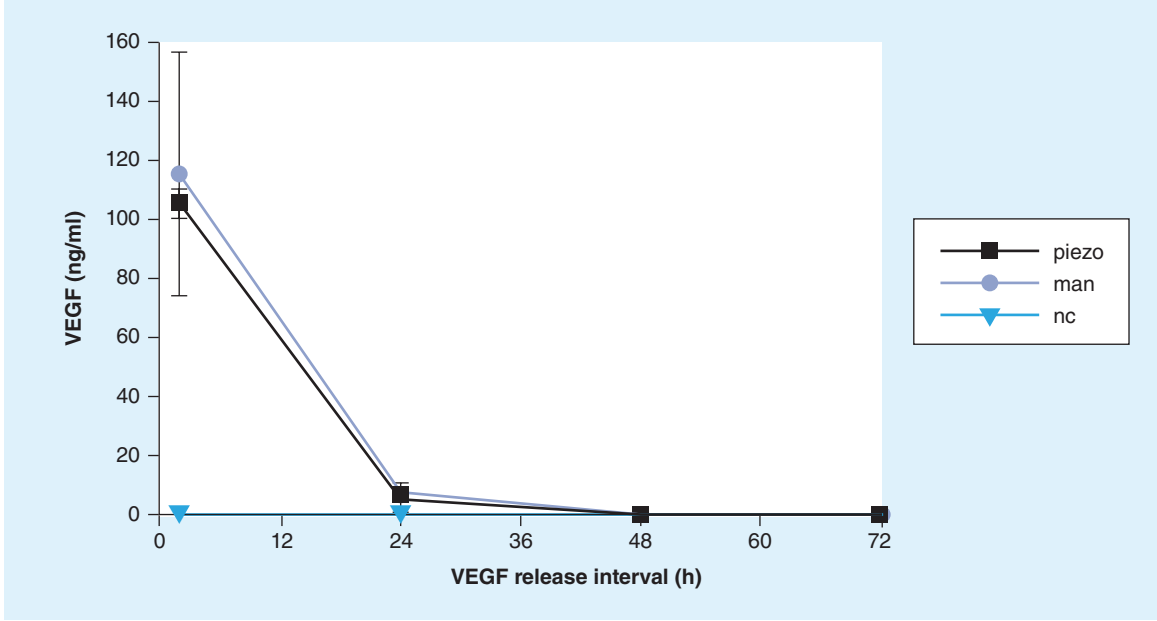

Figure 2. The release kinetics of the samples (piezo: automated piezopipetting, n = 4) and the controls (man: manual pipetting, n = 3) were very similar. Almost all VEGF was released with the initial burst (93% within 2 h). No VEGF was released from the negative control (nc; n = 1).

Executive summary

- Macroscopic extrusion-based 3D printing (3D plotting) was combined with precise microdispensing of liquids enabling localized functionalization of 3D scaffolds during their fabrication.
- By broadening the range of applicable materials and their combinations, the potential for the fabrication of patient individual implants and complex tissue equivalents is enhanced.
- A fluorescein gradient on a 3D scaffold was accomplished by alternating extrusion of calcium phosphate cement strands and pipetting in a layer-by-layer fashion demonstrating the feasibility of the new fabrication strategy.
- Though slower than inkjet printing, the integrated nanoliter pipetting offers the possibility of dispensing an arbitrary number of different liquids on the same scaffold.
- Release kinetics of VEGF was not altered by using piezoelectric pipetting.
- Loading and cell seeding strategies need to be further investigated on the basis of agent–solution/material and cell/material interaction, respectively, to achieve effective local functionalization and good cell adhesion.

Acknowledgements

The authors would like to thank S Brüggemeier for excellent technical assistance.

Financial & competing interests disclosure

The authors thank the Saxon Ministry for Higher Education, Research and the Arts (SMWK, contract No. 4–7531.60/29/24) for financial support. The authors have no other relevant affiliations or financial involvement with any organization or entity with a financial interest in or financial conflict with the subject matter or materials discussed in the manuscript apart from those disclosed.

No writing assistance was utilized in the production of this manuscript.

References

1 Ferris CJ, Gilmore KJ, Wallace GG, in het Panhuis M. Biofabrication: an overview of the approaches used for printing of living cells. *Appl. Microbiol. Biotechnol.* 97(10), 4243–4258 (2013).

2 Derby B. Printing and prototyping of tissues and scaffolds. *Science* 338(6109), 921–926 (2012).

3 Billiet T, Vandenhaute M, Schelfhout J, Van Vlierberghe S, Dubruel P. A review of trends and limitations in hydrogel-rapid prototyping for tissue engineering. *Biomaterials* 33, 6020–6041 (2012).

4 Lode A, Meissner K, Luo Y *et al.* Fabrication of porous scaffolds by three-dimensional plotting of a pasty calcium phosphate bone cement under mild conditions. *J. Tissue Eng. Regen. Med.* 8(9), 682–693 (2014).

5 Kolesky DB, Truby RL, Gladman AS, Busbee TA, Homan KA, Lewis JA. 3D bioprinting of vascularized, heterogeneous cell-laden tissue constructs. *Adv. Mater.* 26, 3124–3130 (2014).

6 Vorndran E, Geffers M, Ewald A, Lemm M, Nies B, Gbureck U. Ready-to-use injectable calcium phosphate bone cement paste as drug carrier. *Acta Biomater.* 9, 9558–9567 (2013).

7 Akkineni AR, Luo Y, Schumacher M, Nies B, Lode A, Gelinsky M. 3D plotting of growth factor loaded calcium phosphate cement scaffolds. *Acta Biomater.* 27, 264–274 (2015).

8 Heinemann S, Roessler S, Lemm M, Ruhnow M, Nies B. Properties of injectable ready-to-use calcium phosphate cement based on water-immiscible liquid. *Acta Biomater.* 9(4), 6199–6207 (2013).

9 McKinney RM, Spillane JT, Pearce GW. Fluorescein diacetate as a reference color standard in fluorescent antibody studies. *Anal. Biochem.* 9(4), 474–476 (1964).

10 Kimball S, Mattis P, GIMP-Team. GNU Image Manipulation Program. (1998–2014). www.gimp.org

11 Knaack S, Lode A, Hoyer B *et al.* Heparin modification of a biomimetic bone matrix for controlled release of VEGF. *J. Biomed. Mater. Res. Part A* 102(10), 3500–3511 (2014).

12 Ahlfeld T, Akkineni AR, Förster Y *et al.* Design and fabrication of complex scaffolds for bone defect healing: combined 3D plotting of a calcium phosphate cement and a growth factor-loaded hydrogel. *Ann. Biomed. Eng.* doi:10.1007/s10439–016–1685–4 (2016) (Epub ahead of print).

13 Gasperini L, Maniglio D, Motta A, Migliaresi C. An electrohydrodynamic bioprinter for alginate hydrogels containing living cells. *Tissue Eng. Part C* 21(2), 123–132 (2014).

14 Schütz K, Placht AM, Paul B, Brueggemeier S, Gelinsky M, Lode A. 3D plotting of a cell-laden alginate/methylcellulose blend: towards biofabrication of tissue engineering constructs with clinically relevant dimensions. *J. Tissue Eng. Regen. Med.* doi:10.1002/term.2058 (2015) (Epub ahead of print).

15 Landers R, Muelhaupt R. Desktop manufacturing of complex objects, prototypes and biomedical scaffolds by means of computer-assisted design combined with computer-guided 3D plotting of polymers and reactive oligomers. *Macromol. Mater. Eng.* 282, 17–21 (2000).

16 Jonczyk R, Timur S, Scheper T, Stahl F. Development of living cell microarrays using non-contact micropipette printing. *J. Biotechnol.* 217, 109–111 (2016).

17 Lode A, Reinstorf A, Bernhardt A, Wolf-Brandstetter C, Koenig U, Gelinsky M. Heparin modification of calcium phosphate bone cements for VEGF functionalization. *J. Biomed. Mater. Res. Part A* 86(3), 749–759 (2008).

Review

Regenerative Medicine

Recreating composition, structure, functionalities of tissues at nanoscale for regenerative medicine

Nanotechnology offers significant potential in regenerative medicine, specifically with the ability to mimic tissue architecture at the nanoscale. In this perspective, we highlight key achievements in the nanotechnology field for successfully mimicking the composition and structure of different tissues, and the development of bio-inspired nanotechnologies and functional nanomaterials to improve tissue regeneration. Numerous nanomaterials fabricated by electrospinning, nanolithography and self-assembly have been successfully applied to regenerate bone, cartilage, muscle, blood vessel, heart and bladder tissue. We also discuss nanotechnology-based regenerative medicine products in the clinic for tissue engineering applications, although so far most of them are focused on bone implants and fillers. We believe that recent advances in nanotechnologies will enable new applications for tissue regeneration in the near future.

First draft submitted: 1 September 2016; Accepted for publication: 18 October 2016; Published online: 25 November 2016

Keywords: biomimetic • drug delivery • FDA-approved products • nanomaterial • nanostructure • nanotechnology • regenerative medicine • tissue regeneration

Emine Alarçin[‡,1,2,3], Xiaofei Guan[‡,1,2,4], Sara Saheb Kashaf[1,2], Khairat Elbaradie[5], Huazhe Yang[1,2], Hae Lin Jang*[,1,2,4] & Ali Khademhosseini**[,1,2,4,6,7]

[1]Division of Biomedical Engineering, Department of Medicine, Biomaterials Innovation Research Center, Harvard Medical School, Brigham & Women's Hospital, Boston, MA 02139, USA

[2]Division of Health Sciences & Technology, Harvard-Massachusetts Institute of Technology, Massachusetts Institute of Technology, Cambridge, MA 02139, USA

[3]Department of Pharmaceutical Technology, Faculty of Pharmacy, Marmara University, Istanbul 34668, Turkey

[4]Wyss Institute for Biologically Inspired Engineering, Harvard University, Boston, MA 02115, USA

[5]Department of Zoology, Faculty of Science, Tanta University, Tanta 31527, Egypt

[6]Department of Bioindustrial Technologies, College of Animal Bioscience & Technology, Konkuk University, Seoul 143–701, Republic of Korea

[7]Department of Physics, King Abdulaziz University, Jeddah 21569, Saudi Arabia

*Author for correspondence: hjang@bwh.harvard.edu

**Author for correspondence: alik@bwh.harvard.edu

[‡]Authors contributed equally

Regenerative medicine aims to restore the function of human tissues and organs by stimulating the intrinsic regenerative capacity of the body by utilizing cells, biomaterials and growth factors [1,2]. Current advances in regenerative medicine have led to the creation of bioengineered tissues and organs that can perform key biological functions. For example, biomimetic tissues including bone, blood vessels, urethra, skin, liver, lung, bladder and trachea transplants have been successfully engineered and implanted *in vivo* [3–10]. Bioengineered tissue constructs can grow and remodel *in vivo* since they are composed of living cells, or can stimulate body cells to migrate and integrate into scaffolding materials.

Currently, by virtue of recent achievements in nanotechnology, the composition and structure of bioengineered tissues are becoming more analogous to natural tissues at the nanoscale, providing a biomimetic niche for cells. The activities of cells depend on biochemical and physical signals from surrounding tissues, and since cells dynamically interact with their local microenvironment at the nanoscale, it is necessary to control properties of engineered tissues at these scale lengths. In addition, nanostructured biomaterials can decrease inflammatory response and increase wound healing in comparison to conventional biomaterials, possibly due to their high surface energy affecting protein adsorption and cell adhesion [11]. In this sense, advanced nanotechnologies for mimicking native tissues can also overcome the disadvantages of using autografts or allografts, such as the risk of immune reaction, infection and disease transmission.

In this paper, we highlight key achievements in the nanotechnology field to recreate the composition, structure and functionality of major tissues and organs, using bio-

Future Medicine part of fsg

mimetic and bio-inspired approaches to improve tissue regeneration. In addition, we report on clinically approved nanotechnology-based regenerative medicine products for tissue engineering applications. By providing an overall view of the recent status of nanotechnology applications in the regeneration of various tissues, we expect that this article will be particularly helpful for those who are investigating the regeneration of complex tissues.

Biomimicking tissue composition at nanoscale

Every tissue in the body has its own nanoscale composition which provides a suitable microenvironment to direct cellular differentiation toward a particular lineage. Since engineered nano-architecture features a high surface area to volume ratio, it can systematically expose cells to multiple biological components with different functionalities. The ability to control the spatial distribution of materials at the nanoscale can also enhance tissue regeneration by enabling better integration with host tissue [12]. For example, bone tissue is mainly composed of inorganic calcium phosphate nanocrystals and organic components (mainly collagen type I) [13–15]. It is reported that a nanocomposite scaffold that is composed of both organic and inorganic components of bone tissues can promote bone regeneration [16,17]. In addition, the inorganic phase of human bone tissue is composed of two major bone minerals: hydroxyapatite (HAP: $Ca_{10}[PO_4]_6[OH]_2$) and whitlockite (WH: $Ca_{18}Mg_2[HPO_4]_2[PO_4]_{12}$) nanocrystallites, with different physicochemical properties [14,15]. For example, Mg^{2+} ions are too small in size to maintain a HAP crystal structure, and so are mostly incorporated in the WH crystal structure [14,18]. Furthermore, it is reported that these two bone crystals are distributed in different ratios depending on certain regions of bone tissue [14], implying that HAP and WH have distinguished biological roles. Therefore, controlling their spatial distribution at the nanoscale is important for mimicking native bone tissue.

In Table 1, we have listed representative examples of recent research achievements to recreate the nanoscale composition of each tissue type. However, despite many outstanding achievements in both the nanotechnology and tissue engineering fields, so far, most bioengineered tissues are still dependent on the usage of bulk materials with micrometer scale designs or larger, which have limited tissue functions. Therefore, there remains a strong need to further develop nanomaterials that mimic the major components of tissues at the nanoscale and apply them for tissue regeneration.

Mimicking nanoscale tissue structure

Human tissues have complex topographical features at the nanoscale that can physically influence the behavior of cells by directly modulating their migration, orientation, differentiation and proliferation. For example, skeletal and cardiac muscles are composed of perpendicularly interwoven collagen strips and elastin bundles at the nanometer scale [28]. Also, bone tissue is composed of HAP nanocrystals that form nanopatterns along collagen fibers [29]. In addition, highly connected nanopores/channels in tissues can continuously supply a sufficient level of oxygen and nutrients to cells, and allow for intercommunication between different cell types. For example, there exist three levels of hierarchical pore architectures within cortical and cancellous bone, ranging from 10 to 20 μm in radii, which support blood or interstitial fluid transportation [30].

To mimic the nanoscale structure of each tissue type to stimulate cells with the proper topographical cues, nanofibrous and nanocomposite structures, nanoscale surface topographies and nanoporous/nanochannel networks in the scaffold have been engineered by nanotechnologies such as electrospinning, nanolithography, self-assembly, phase separation and sacrificial template methods (Table 2).

Since the cellular microenvironment includes ECM components such as fibril structured proteins and polysaccharides [43], engineered nanofiber networks can support cellular growth and regulate cellular behaviors in a physiologically similar manner [44]. Aligned nanofibers are especially useful in guiding cellular orientation to mimic the anisotropy of natural tissues, including heart, nerve, tendon and blood vessels. For example, when human tendon progenitor cells were seeded on aligned poly (L-lactic acid) nanofibers that recapitulated parallel collagen fibers in tendon, these cells expressed higher level of tendon specific genes compared with cells grown on random fibers [34].

Nanocomposite structures are used widely, as they can enhance the mechanical strength of hybrid organic/inorganic composites, and thus influence cellular proliferation and differentiation. To mimic the organization of bone tissue that is composed of inorganic minerals and organic collagen matrix, silicate nanoparticles were incorporated into organic materials, enhancing mechanical properties (i.e., compressive strength, tensile strength and elastic modulus) and further promoting cellular proliferation [37,38,45]. In fact, stiffness is one of the key parameters for altering cell growth and differentiation [46,47]. Recently, Alakpa *et al.* fabricated supramolecular nanofiber hydrogels and controlled their stiffness to direct the differentiation of stem cells without any biochemical functionalization [47].

Table 1. Examples of biomimicking composition of tissues at nanoscale.

Tissue	Nanotechnologies	Functionality	Tissue regeneration capacity	Ref.
Bone	Hydroxyapatite composite sponge with concentrated collagen nanofibers	Mimicking bone chemistry based on osteoconductive scaffolds composed of inorganic material and natural polymers	Induced continuous deposition of lamellar bone tissue while maintaining osteoblast activity	[17]
	Synthesis of the two major bone crystals: hydroxyapatite and whitlockite nanoparticles	Mimicking inorganic composition of bone, providing mechanical stability and stimulating osteogenic differentiation of stem cells	Enhanced proliferation and differentiation of bone cells and induced rapid regeneration of bone tissues	[19,20]
	Self-assembled peptide amphiphile nanofibrous matrices to induce biomimetic nucleation of hydroxyapatite crystals	Mimicking bone mineralization with collagen-like fibril structure and nucleation of hydroxyapatite crystals	Promoted new bone formation in a rat femoral defect model	[21]
Cartilage	Peptide amphiphilic nanofibers functionalized with chemical groups of GAG molecules	Mimicking composition, structure and function of the ECM	Enhanced aggregation of MSCs and deposition of cartilage-specific matrix elements	[22]
	Self-assembled supramolecular GAGs like glycopeptide nanofibers	Mimicking composition and functions of HA, the major component of cartilage	Induced chondrogenic differentiation of MSCs and enhanced formation of hyaline-like cartilage	[23]
Heart	Nanofibrous collagen scaffold made by electrospinning and crosslinking for cardiac tissue regeneration	Mimicking composition of myocardial connective stroma and delivery of cardiomyocytes	Improved vascularization of scaffold with upregulation of gene expression related to ECM remodeling, after implanted *in vivo*	[24]
	MSC seeded polycaprolactone nanofiber cardiac patch by fibronectin immobilization	Mimicking ECM of heart by using fibronectin, which is a major component of normal heart for cell adhesion and activity	Enhanced cellular adhesion increased angiogenesis, and improved cardiac function	[25]
Skin	Multilayer nanofilm composed of HA and poly-L-lysine on top of a HA scaffold by using layer-by-layer assembly for skin tissue engineering	Mimicking epidermal–dermal composition and structure of skin at nanometer scale	Promoted adhesion of keratinocytes, enhancing epidermal protective barrier function of skin	[26]
Muscle	Laminin mimetic peptide nanofibrous network	Mimicking composition and structure of skeletal muscle basal lamina	Enhanced cellular gene expression related to skeletal muscle specific marker	[27]

ECM: Extracellular matrix; GAG: Glycosaminoglycan; HA: Hyaluronic acid; MSC: Mesenchymal stem cell.

Nanopatterns play an important role in directing various cellular behaviors, due to their structural consistency with many vital components of native ECM, such as basement membrane and focal adhesion complexes, ranging from a few to a hundred nanometers [48,49]. Patterning techniques at the nanoscale allow for the mimicking of native ECM, thus modulating cell-matrix interactions [50]. Interestingly, nanoscale disorders can direct osteogenic differentiation of human MSCs in the absence of osteogenic supplements [40]. On the other hand, when the pattern contains absolute square lattice symmetry, nanoscale patterning can also promote the growth of stem cells and the retention of multipotency, indicating that nanoscale surface topographies can determine cell fate and functions [41]. Likewise, since cell orientation strongly correlates with the direction of underneath patterns, nanoscale structural cues can further control the macroscopic function of tissue constructs. For example, nanotopographically controlled heart tissue constructs that mimic the ECM structure of myocardium have successfully demonstrated anisotropic action potential conduction and contractility characteristics of native cardiac tissue [39].

Nanopores/channels in natural tissues are also vital for maintaining the activity of cells, as they provide transport paths for oxygen and nutrients [51,52]. While it seems that the two concepts of permeability

Table 2. Examples of mimicking nanoscale tissue structure for tissue regeneration.

Nanostructure	Tissue	Nanotechnology	Tissue regeneration capacity	Ref.
Nanofibrous structures	Heart	Electrospun aligned poly(lactide)- and poly(glycolide)-based scaffold	Demonstrated directionally dependent mature contractile machinery of cardiomyocytes and increased their synchronized beating	[31]
		Highly aligned nanofiber engineered by rotary jet spinning	Induced alignment of rat ventricular myocytes along with the nanofiber	[32,33]
	Tendon	Electrospun aligned PLLA nanofibers	Upregulated tendon-specific genes	[34]
	Cartilage	Nanofibrous hollow microspheres with ECM mimetic architecture as an injectable cell carrier	Induced successful cartilage regeneration in a critical-size osteochondral defect in a rabbit model	[35]
	Skin	3D Multilayered nanofibrous scaffold	Produced dermal-like tissues or bilayer skin tissues with both epidermal and dermal layers	[36]
Nanocomposite structures	Bone	Nanocomposite made from poly(ethylene oxide) and silicate nanoparticles	Induced direction-dependent mechanical properties with increased mechanical strength and extensibility, enhancing cellular activities and mineralization	[37,38]
Nanotopographies	Heart	Myocardium model with controlled nanoscale surface topographies mimicking function of mayocardial tissue and ECM architecture	Displayed anisotropic action potential conduction and contraction of native cardiac tissues	[39]
	Bone	Nanostructured surfaces with symmetry or disorder to modulate stem cell differentiation	Enabled to control MSCs to maintain multipotency or to produce bone minerals depending on nanopatterns	[40,41]
Nanoporous/ nanochannel structures	Bone	Self-assembled hierarchical nanochannel network in bone ceramic	Provided both sufficient mechanical strength and efficient nutrient supply for bone cell growth and differentiation	[42]
	Vessel	Nanopores in the vessel wall mimicking a vascular bed	Enhanced permeability and intercellular crosstalk	[4]

ECM: Extracellular matrix; MSC: Mesenchymal stem cell; PLLA: Poly(L-lactic acid).

and mechanical strength are contradictory, as they are directly or inversely correlated with the porosity of the structures, nanoporous/channel structures can simultaneously satisfy these properties due to their enhanced permeability compared with microporous/channel structures. In fact, the amount of nutrients that are delivered by nanochannels is known to be sufficient to sustain cellular vital activities. Nanopores/channels have been incorporated in vascularized cardiac or hepatic tissue constructs and bone scaffolds by using self-assembled and porogen methods to enhance permeability and permit cellular crosstalk, while maintaining mechanical properties [4,42].

Developing bioinspired nanotechnologies & functional nanomaterials

The function of human tissue occurs based on the localized microenvironment where cells interact with specific types of ECM at the nanoscale. In this respect, nanoscale delivery systems and functional nanomaterials have been applied for directing cellular differentiation and tissue specific activities to restore function of damaged tissues.

In the past two decades, nanoscale delivery systems have attracted a great deal of attention by researchers in the field of regenerative medicine based on their unique features, such as high surface area and easiness of surface functionalization, which can promote the adsorption of growth factors and drugs [53,54]. For example, nanofibers are one of the most widely used nanoscale delivery platforms based on their similarity with the physical structure of ECM [55,56]. Hartgerink *et al.* developed an injectable, self-assembled peptide-based nanofibrous hydrogel that contains peptides for pro-angiogenic moieties which can rapidly form mature vascular networks and induce tissue integration after subcutaneous delivery *in vivo* via a syringe needle [56].

Functional nanomaterials can actively support damaged tissues with functional loss, and thus can enhance their regeneration. For example, electroconductive

Table 3. Developing bioinspired nanotechnologies and functional nanomaterials for tissue regeneration.

Tissue	Nanotechnologies	Functionality	Tissue regeneration capacity	Ref.
Bone	Biomimetic ECM nanostructures constructed through layer-by-layer self-assembly of biodegradable nanoparticles and polysaccharides	Preservation of the activity of osteoinductive growth factors and induced their sustained release	Promoted the attachment, proliferation and differentiation of BMSCs and enhanced new bone formation by sustained release of biomolecules	[60]
	Intermediate precursors-loaded mesoporous silica nanoparticles as delivery devices for biomineralization	Sustained release of amorphous calcium phosphate precursors	Induced biomimetic intrafibrillar mineralization of collagen	[61]
Cartilage	ECM mimetic chondroitin sulfate/polyethylene glycol/GO hybrid nanocomposite scaffold for cartilage engineering	Improvement of overall mechanical properties and electrical conductivity of scaffold by GO	Enhanced regeneration of cartilage tissue with improved subchondral bone reconstruction	[62]
	Bioprinted nanoliter droplets encapsulating stem cells and growth factors to mimic native fibrocartilage microenvironment	Mimicking the complex anisotropic fibrocartilage tissue by 3D printing nanoliter droplets encapsulating MSCs along with biochemical gradient and ECM components	Upregulated osteogenic and chondrogenic related genes in the 3D fibrocartilage model	[63]
	Self-assembled supramolecular peptide amphiphile nanofibers containing binding epitopes to TGF-β-1 for cartilage regeneration	Prolonged release of TGF-β-1 from PA gels containing high density of TGFβ-1 binding sites	Promoted articular cartilage regeneration in a rabbit chondral defect model without any exogenous growth factor	[64]
Vessels	VEGF-loaded heparin-functionalized PLGA nanoparticle–fibrin gel complex	Localized and sustained delivery of growth factor	Improved the therapeutic angiogenic effect in an ischemic hind limb model by increasing blood pressure, angiographic score and the capillary density	[65]
	Biodegradable porous silicon nanoneedles for local intracellular delivery of nucleic acids to induce tissue neovascularization	Codelivery of DNA and siRNA into cell cytosol by nano-injection	Induced localized neovascularization and increased blood perfusion *in vivo*	[66]
	Peptide amphiphile nanostructures that display VEGF mimetic peptide on the surface of nanofibers	Mimicking the activity of VEGF by generating phosphorylation of VEGF receptors	Enhanced proangiogenic activities of endothelial cells and microcirculatory angiogenesis in the ischemic tissue	[67]
Heart	Pluripotent stem cell-derived cardiomyocyte spheroids that incorporate electrically conductive silicon nanowires	Formation of electrically conductive microenvironment in cardiac spheroids which can synergize with exogenous electrical stimulation	Enhanced cell–cell junction formation, increased contractile machinery expression, while regulating the endogenous spontaneous beating of pluripotent stem-cell-derived cardiac spheroids	[57]
	Hybrid hydrogel scaffold incorporating aligned carbon nanotubes	Tunable and anisotropic mechanical and electrical characteristics	Enhanced cardiac differentiation of embryoid bodies with increased beating activity	[58]
Bladder	PLGA nanoparticle thermosensitive gel scaffold for bladder tissue regeneration	Codelivery of growth factors by a PLGA nanoparticle carrier	Promoted bladder tissue regeneration with rapid vascularization while inhibiting graft contracture in a rabbit model	[9]
Nerves	PLGA nanoparticles including LIF as a cargo with surface modification to target OPCs for myelin repair	Sustained and controlled release of LIF by PLGA nanoparticles after selectively attached to OPCs	Induced remyelination with increased myelinated axon numbers and myelin thickness per axon	[68]

BMSC: Bone marrow stem cell; ECM: Extracellular matrix; GO: Graphene oxide; MSC: Mesenchymal stem cell; OPC: Oligodendrocyte precursor cell; PA: Peptide amphiphile; PLGA: Poly(D,L-lactic-co-glycolic acid).

Table 4. Selective list of FDA approved nanotechnology products for tissue regeneration.

Name/company	Approved applications	Product description	Function and clinical outcomes	US FDA approval year	Ref.
Vitoss® scaffold synthetic cancellous bone void filler/Stryker Corporation	Filler, osseous defects	Highly porous 3D β-tricalcium phosphate scaffold based on calcium phosphate nanoparticles	This filler has similar composition to natural bone minerals, enhancing bone regeneration, along with increased spinal fusion rates	2003	[70–72]
Ostim® bone grafting material/Heraeus Kulzer, Inc.	Filler, osseous defects	Nanocrystalline hydroxyapatite paste that is injected into a bone void or defect	This filler facilitates bone regeneration, based on its bone mimetic chemical composition and crystalline structures	2004	[70,73]
NanOss™ bone void filler/Angstrom Medica, Inc.	Filler, osseous defects	Osteoconductive, resorbable bone graft that uses calcium phosphate nanocrystals	This dense, nanocrystalline material mimics the microstructure and composition of bone and has strong mechanical properties and osteoconductive effects	2005	[74,75]
BoneGen-TR/BioLok International, Inc.	Filler, oral surgery, periodontics, endodontics, implantology	Calcium sulfate-based nanocomposite	The filler can control timed release of calcium sulfate that supports bone augmentation	2006	[76]
EquivaBone osteoinductive bone graft substitute/ETEX Corporation	Filler, osseous defects	Resorbable, osteoinductive bone graft substitute that is composed of demineralized bone matrix and nanocrystalline hydroxyapatite	This scaffold has osteoconductive effect by providing hydroxyapatite nanocrystalline and osteoinductive growth factors	2009	[77,78]
Beta-BSM injectable bone substitute material/ETEX Corporation	Filler, osseous defects	Synthetic calcium phosphate bone graft material in a nanocrystalline matrix	This filler has osteoconductive properties based on bone mimetic chemical structure	2010	[78]
NanoGen/Orthogen, LLC	Filler, osseous defects	Medical grade calcium sulfate hemihydrate based nanocomposite	This filler is controlled to be degraded over a period of 12 weeks, stimulating bone regeneration	2011	[79]
FortiCore™/Nanovis, Inc.	Implant, spinal fusion procedures	Implant composed of a highly porous titanium scaffold that is integrated with a PEEK-OPTIMA (high-performance, implant-grade polymer) core	This implant has nanotube-enhanced surface which can promote bone regeneration around the implant	2014	[80]
NB3D bone void filler/ Pioneer Surgical Technology, Inc.	Filler, osseous defects	3D construct that is composed of porous hydroxyapatite nanogranules suspended in a porous gelatin-based foam matrix	This filler has interconnected porosity similar to human cancellous bone and also has equivalent crystal size and structure as natural bone, promoting tissue interaction and regeneration	2014	[81]

nanomaterials have been applied for the treatment of cardiac tissues to generate electrical function of these tissues. The incorporation of electrically conductive silicon nanowires in cardiac spheroids can provide an endogenous electrical microenvironment for cardiomyocytes, and synergize with exogenous electrical

stimulation, enhancing cardiac microtissue development [57]. In addition, when carbon nanotubes are integrated into hydrogels and oriented in an aligned manner, the cardiac differentiation of embryoid bodies and their beating activities are enhanced. The incorporation of carbon nanotubes in a hydrogel scaffold has been reported to further enhance the mechanical properties of tissue constructs [58]. The functionalization of biomaterials by the internalization of biological motifs can also control cellular behavior; for instance, Gouveia *et al.* incorporated peptide amphiphile composed of the N-(fluorenyl-9-methoxycarbonyl) (Fmoc) molecule linked to the cell-adhesion Arg–Gly–Asp–Ser (RGDS) motif into biomimetic collagen gels. These functionalized hydrogels promoted attachment and proliferation of human corneal stromal fibroblasts [59].

In Table 3, we have listed representative examples of the current use of nanotechnologies and nanomaterials to enhance tissue regeneration.

FDA approved regenerative medicine products for tissue regeneration based on nanotechnologies

In the 2014 Guidance for Industry entitled "Considering Whether an FDA-Regulated Product Involves the Application of Nanotechnology," the US FDA defined nanotechnology products as those which have at least one dimension between 1 and 100 nm in size [69]. The FDA also recognized materials that are as large as 1000 nm as nanomaterials if they can demonstrate similar 'properties or phenomena' as other nanotechnology-based products [69]. During the process of commercialization, a nanotechnology product moves through various developmental phases, starting with the basic concept product and culminating with clinical investigations and commercialization. The resulting nanotechnology products can belong to various FDA classifications, such as biologicals, devices, genetics, drugs and others [70].

Based on recent achievements in nanotechnologies for recreating the composition, structure and functions of tissues in a more precise way than ever before, the related nanotechnologies are starting to be applied in clinics to repair diseased/damaged tissues [2,70]. In Table 4, we have selectively listed nanotechnology based products for tissue regeneration that have obtained approval from FDA and are currently on the market.

Conclusion & future perspective

In this special issue, we selectively highlighted state-of-the-art nanotechnologies that successfully mimic the composition and structure of different tissue types, as well as bio-inspired nanotechnologies and functional nanomaterials for tissue regeneration. Based on recent advances in nanotechnologies and tissue engineering, bioengineered tissues are becoming more similar to natural tissues, thus enabling the partial recovery of damaged/diseased tissues. However, there are still many biological components that are not fully understood or ignored in regenerative medicine due to the

Executive summary

- This paper highlights the key achievements in the nanotechnology field for regenerative medicine to recreate functional biomimetic tissues and organs.

Biomimicking tissue composition at nanoscale

- Every tissue in the body has its own nanoscale composition.
- Controlling nanoscale composition is important as each tissue type has a unique spatial distribution of materials at the nanoscale which then provides different types of niches for cells.

Mimicking nanoscale tissue structure

- Human tissues have complex topographical features at the nanoscale.
- Nanofibrous and nanocomposite structures, nanotopographies and nanoporous/nanochannel structures have been designed and built by utilizing nanotechnologies such as electrospinning, nanolithography, self-assembly, phase separation and sacrificial template method.

Developing bioinspired nanotechnologies & functional nanomaterials

- Nanoscale delivery systems have provided the sustained and controlled release of growth factors for tissue regeneration.
- Functional nanomaterials have successfully generated similar or even better tissue functions to stimulate cells to repair tissues.

US FDA approved clinical products for regenerative medicine based on nanotechnologies

- Recently, FDA approved nanotechnology based regenerative medicine products have started to be actively used in the clinic for tissue regeneration.
- Most of the current nanotechnology based regenerative medicine products are made for bone tissue regeneration.
- We anticipate that the recent achievements in the nanotechnology field will further lead to the development of regenerative medicine products for various tissue types in the near future.

difficulty in their fabrication. Moreover, although many nanomaterials can successfully promote cellular activities *in vitro*, there still exist safety concerns about the use of these nanomaterials, as they can cause systemic side effects by crossing cell barriers in non-targeted organs. In fact, most of the newly developed nanomaterials have not been assessed in large animal models. As a result, except for bone related materials, the majority of the newly developed nanomaterials have not been applied for tissue regeneration in the clinic. These issues can be addressed by thorough physicochemical characterization of nanomaterials and restriction of undesired uptake via functionalization with targeting moieties [82,83]. Based on the understanding of the effectiveness and safety of nanomaterials, proper *in vivo* studies should be continued with selective nanomaterials for the purpose of clinical translation. We envision that the development of nanotechnologies, which is becoming faster than ever before, will overcome current challenges in regenerative medicine to heal diseased/damaged tissues in the near future.

Financial & competing interests disclosure

The authors gratefully acknowledge funding from the NIH (AR057837, AR070647), and the Presidential Early Career Award for Scientists and Engineers (PECASE). Emine Alarçin was supported by post-doctoral research grant of The Scientific and Technological Research Council of Turkey (TUBITAK). The authors have no other relevant affiliations or financial involvement with any organization or entity with a financial interest in or financial conflict with the subject matter or materials discussed in the manuscript apart from those disclosed.

No writing assistance was utilized in the production of this manuscript.

References

Papers of special note have been highlighted as:
• of interest; •• of considerable interest

1 Mason C, Dunnill P. A brief definition of regenerative medicine. *Regen. Med.* 3(1), 1–5 (2008).

2 Engel E, Michiardi A, Navarro M, Lacroix D, Planell JA. Nanotechnology in regenerative medicine: the materials side. *Trends Biotechnol.* 26(1), 39–47 (2008).

3 Sun D, Chen Y, Tran RT *et al.* Citric acid-based hydroxyapatite composite scaffolds enhance calvarial regeneration. *Sci. Rep.* 4 6912 (2014).

4 Zhang B, Montgomery M, Chamberlain MD *et al.* Biodegradable scaffold with built-in vasculature for organ-on-a-chip engineering and direct surgical anastomosis. *Nat. Mater.* 15(6), 669–678 (2016).

• **Nanopores' structure is incorporated in vascularized cardiac or hepatic tissue and bone scaffolds.**

5 Jia W, Tang H, Wu J *et al.* Urethral tissue regeneration using collagen scaffold modified with collagen binding VEGF in a beagle model. *Biomaterials* 69, 45–55 (2015).

6 Yu B, Kang S-Y, Akthakul A *et al.* An elastic second skin. *Nat. Mater.* 15(8), 911–918 (2016).

7 Mazza G, Rombouts K, Hall AR *et al.* Decellularized human liver as a natural 3D-scaffold for liver bioengineering and transplantation. *Sci. Rep.* 5, 1–15 (2015).

8 Ren X, Moser PT, Gilpin SE *et al.* Engineering pulmonary vasculature in decellularized rat and human lungs. *Nat. Biotechnol.* 33(10), 1097–1102 (2015).

9 Jiang X, Lin H, Jiang D *et al.* Co-delivery of VEGF and bFGF via a PLGA nanoparticle-modified BAM for effective contracture inhibition of regenerated bladder tissue in rabbits. *Sci. Rep.* 6, 1–12 (2016).

10 Jungebluth P, Haag JC, Sjöqvist S *et al.* Tracheal tissue engineering in rats. *Nat. Protoc.* 9(9), 2164–2179 (2014).

11 Ainslie KM, Thakar RG, Bernards DA, Desai TA. Inflammatory response to implanted nanostructured materials. In: *Biological Interactions on Materials Surfaces*. Puleo DA, Bizios R (Eds). Springer, New York, USA, 355–371 (2009).

• **This book chapter discusses advantages of nanostructured biomaterials in inflammatory response.**

12 Perez RA, Won J-E, Knowles JC, Kim H-W. Naturally and synthetic smart composite biomaterials for tissue regeneration. *Adv. Drug Del. Rev.* 65(4), 471–496 (2013).

13 Wang Y, Azaïs T, Robin M *et al.* The predominant role of collagen in the nucleation, growth, structure and orientation of bone apatite. *Nat. Mater.* 11(8), 724–733 (2012).

14 Driessens FC, Verbeeck R. *Biominerals.* CRC Press, USA (1990).

15 Elliott JC. Structure and chemistry of the apatites and other calcium orthophosphates. In: *Studies In Organic Chemistry.* Elsevier, Amsterdam, The Netherlands (1994).

16 Kikuchi M. Hydroxyapatite/collagen bone-like nanocomposite. *Biol. Pharm. Bull.* 36(11), 1666–1669 (2013).

17 Scaglione S, Giannoni P, Bianchini P *et al.* Order versus disorder: *in vivo* bone formation within osteoconductive scaffolds. *Sci. Rep.* 2, 1–6 (2012).

18 Terpstra R, Driessens F. Magnesium in tooth enamel and synthetic apatites. *Calcif. Tissue Int.* 39(5), 348–354 (1986).

19 Jang HL, Jin K, Lee J *et al.* Revisiting whitlockite, the second most abundant biomineral in bone: nanocrystal synthesis in physiologically relevant conditions and biocompatibility evaluation. *ACS Nano* 8(1), 634–641 (2013).

•• **Reports a facile synthetic methodology for the second major bone mineral in the human body.**

20 Jang HL, Zheng GB, Park J *et al. In vitro* and *in vivo* evaluation of whitlockite biocompatibility: comparative study with hydroxyapatite and β-tricalcium phosphate. *Adv. Healthc. Mater.* 5(1), 128–136 (2015).

21 Mata A, Geng Y, Henrikson KJ *et al.* Bone regeneration mediated by biomimetic mineralization of a nanofiber matrix. *Biomaterials* 31(23), 6004–6012 (2010).

22 Yaylaci SU, Sen M, Bulut O, Arslan E, Guler MO, Tekinay AB. Chondrogenic differentiation of mesenchymal stem cells on glycosaminoglycan-mimetic peptide nanofibers. *ACS Biomater. Sci. Eng.* 2(5), 871–878 (2016).

23 Ustun Yaylaci S, Sardan Ekiz M, Arslan E *et al.* Supramolecular GAG-like Self-assembled glycopeptide nanofibers induce chondrogenesis and cartilage regeneration. *Biomacromolecules* 17(2), 679–689 (2016).

24 Joanne P, Kitsara M, Boitard S-E *et al.* Nanofibrous clinical-grade collagen scaffolds seeded with human cardiomyocytes induces cardiac remodeling in dilated cardiomyopathy. *Biomaterials* 80 157–168 (2016).

25 Kang B-J, Kim H, Lee SK *et al.* Umbilical-cord-blood-derived mesenchymal stem cells seeded onto fibronectin-immobilized polycaprolactone nanofiber improve cardiac function. *Acta Biomater.* 10(7), 3007–3017 (2014).

26 Monteiro IP, Shukla A, Marques AP, Reis RL, Hammond PT. Spray-assisted layer-by-layer assembly on hyaluronic acid scaffolds for skin tissue engineering. *J. Biomed. Mater. Res. A* 103(1), 330–340 (2015).

27 Yasa IC, Gunduz N, Kilinc M, Guler MO, Tekinay AB. Basal lamina mimetic nanofibrous peptide networks for skeletal myogenesis. *Sci. Rep.* 5, 16460 (2015).

28 Parker KK, Ingber DE. Extracellular matrix, mechanotransduction and structural hierarchies in heart tissue engineering. *Philos. Trans. R. Soc. Lond. B Biol. Sci.* 362(1484), 1267–1279 (2007).

29 Dvir T, Timko BP, Kohane DS, Langer R. Nanotechnological strategies for engineering complex tissues. *Nat. Nanotechnol.* 6(1), 13–22 (2011).

30 Cowin SC, Cardoso L. Blood and interstitial flow in the hierarchical pore space architecture of bone tissue. *J. Biomech.* 48(5), 842–854 (2015).

31 Zong X, Bien H, Chung C-Y *et al.* Electrospun fine-textured scaffolds for heart tissue constructs. *Biomaterials* 26(26), 5330–5338 (2005).

32 Badrossamay MR, Balachandran K, Capulli AK *et al.* Engineering hybrid polymer-protein super-aligned nanofibers via rotary jet spinning. *Biomaterials* 35(10), 3188–3197 (2014).

33 Badrossamay MR, Mcilwee HA, Goss JA, Parker KK. Nanofiber assembly by rotary jet-spinning. *Nano Lett.* 10(6), 2257–2261 (2010).

34 Yin Z, Chen X, Chen JL *et al.* The regulation of tendon stem cell differentiation by the alignment of nanofibers. *Biomaterials* 31(8), 2163–2175 (2010).

35 Liu X, Jin X, Ma PX. Nanofibrous hollow microspheres self-assembled from star-shaped polymers as injectable cell carriers for knee repair. *Nat. Mater.* 10(5), 398–406 (2011).

36 Yang X, Shah JD, Wang H. Nanofiber enabled layer-by-layer approach toward three-dimensional tissue formation. *Tissue Eng. Pt. A* 15(4), 945–956 (2008).

37 Gaharwar AK, Schexnailder PJ, Kline BP, Schmidt G. Assessment of using Laponite® cross-linked poly (ethylene oxide) for controlled cell adhesion and mineralization. *Acta Biomater.* 7(2), 568–577 (2011).

38 Gaharwar AK, Schexnailder P, Kaul V *et al.* Highly extensible bio-nanocomposite films with direction-dependent properties. *Adv. Funct. Mater.* 20(3), 429–436 (2010).

39 Kim D-H, Lipke EA, Kim P *et al.* Nanoscale cues regulate the structure and function of macroscopic cardiac tissue constructs. *Proc. Natl Acad. Sci. USA* 107(2), 565–570 (2010).

40 Dalby MJ, Gadegaard N, Tare R *et al.* The control of human mesenchymal cell differentiation using nanoscale symmetry and disorder. *Nat. Mater.* 6(12), 997–1003 (2007).

41 Mcmurray RJ, Gadegaard N, Tsimbouri PM *et al.* Nanoscale surfaces for the long-term maintenance of mesenchymal stem cell phenotype and multipotency. *Nat. Mater.* 10(8), 637–644 (2011).

42 Jang HL, Lee K, Kang CS *et al.* Biofunctionalized ceramic with self-assembled networks of nanochannels. *ACS Nano* 9(4), 4447–4457 (2015).

43 Pellowe AS, Gonzalez AL. Extracellular matrix biomimicry for the creation of investigational and therapeutic devices. *Wiley Interdiscip. Rev. Nanomed. Nanobiotechnol.* 8(1), 5–22 (2016).

44 Liu W, Thomopoulos S, Xia Y. Electrospun nanofibers for regenerative medicine. *Adv. Healthc. Mater.* 1(1), 10–25 (2012).

45 Asran AS, Henning S, Michler GH. Polyvinyl alcohol–collagen–hydroxyapatite biocomposite nanofibrous scaffold: mimicking the key features of natural bone at the nanoscale level. *Polymer* 51(4), 868–876 (2010).

46 Caiazzo M, Okawa Y, Ranga A, Piersigilli A, Tabata Y, Lutolf MP. Defined three-dimensional microenvironments boost induction of pluripotency. *Nat. Mater.* 15(3), 344–352 (2016).

47 Alakpa EV, Jayawarna V, Lampel A *et al.* Tunable supramolecular hydrogels for selection of lineage-guiding metabolites in stem cell cultures. *Chem* 1(2), 298–319 (2016).

48 Stevens MM, George JH. Exploring and engineering the cell surface interface. *Science* 310(5751), 1135–1138 (2005).

49 Geiger B, Bershadsky A, Pankov R, Yamada KM. Transmembrane crosstalk between the extracellular matrix and the cytoskeleton. *Nat. Rev. Mol. Cell Biol.* 2(11), 793–805 (2001).

50 Rahmany MB, Van Dyke M. Biomimetic approaches to modulate cellular adhesion in biomaterials: a review. *Acta Biomater.* 9(3), 5431–5437 (2013).

51 West GB, Brown JH. The origin of allometric scaling laws in biology from genomes to ecosystems: towards a quantitative unifying theory of biological structure and organization. *J. Exp. Biol.* 208(9), 1575–1592 (2005).

52 Banavar JR, Maritan A, Rinaldo A. Size and form in efficient transportation networks. *Nature* 399(6732), 130–132 (1999).

53 Perán M, García MA, López-Ruiz E *et al.* Functionalized nanostructures with application in regenerative medicine. *Int. J. Mol. Sci.* 13(3), 3847–3886 (2012).

54 Zhang L, Webster TJ. Nanotechnology and nanomaterials: promises for improved tissue regeneration. *Nano Today* 4(1), 66–80 (2009).

55 James R, Laurencin CT. Nanofiber technology: its transformative role in nanomedicine. *Nanomedicine (Lond.)* 11(12), 1499–1501 (2016).

56 Kumar VA, Taylor NL, Shi S *et al.* Highly angiogenic peptide nanofibers. *ACS Nano* 9(1), 860–868 (2015).

• **This minimally invasive injectable hydrogel significantly enhances the formation of robust mature vascular networks in a rat model.**

57 Richards DJ, Tan Y, Coyle R *et al.* Nanowires and electrical stimulation synergistically improve functions of hiPSC cardiac spheroids. *Nano Lett.* 16(7), 4670–4678 (2016).

58 Ahadian S, Yamada S, Ramón-Azcón J *et al.* Hybrid hydrogel-aligned carbon nanotube scaffolds to enhance cardiac differentiation of embryoid bodies. *Acta Biomater.* 31, 134–143 (2016).

59 Gouveia RM, Jones RR, Hamley IW, Connon CJ. The bioactivity of composite Fmoc-RGDS-collagen gels. *Biomater. Sci.* 2(9), 1222–1229 (2014).

60 Wang Z, Dong L, Han L *et al.* Self-assembled Biodegradable Nanoparticles and Polysaccharides as Biomimetic ECM Nanostructures for the Synergistic effect of RGD and BMP-2 on Bone Formation. *Sci. Rep.* 6, 25090 (2016).

61 Zhang W, Luo X-J, Niu L-N *et al.* Biomimetic intrafibrillar mineralization of type I collagen with intermediate precursors-loaded mesoporous carriers. *Sci. Rep.* 5, 11199 (2015).

62 Liao J, Qu Y, Chu B, Zhang X, Qian Z. Biodegradable CSMA/PECA/graphene porous hybrid scaffold for cartilage tissue engineering. *Sci. Rep.* 5, 9879 (2015).

• **This delivery strategy significantly enhances continuous subchondral bone formation and thicker newly formed cartilage in a rabbit model.**

63 Gurkan UA, El Assal R, Yildiz SE *et al.* Engineering anisotropic biomimetic fibrocartilage microenvironment by bioprinting mesenchymal stem cells in nanoliter gel droplets. *Mol. Pharm.* 11(7), 2151–2159 (2014).

64 Shah RN, Shah NA, Lim MMDR, Hsieh C, Nuber G, Stupp SI. Supramolecular design of self-assembling nanofibers for cartilage regeneration. *Proc. Natl Acad. Sci. USA* 107(8), 3293–3298 (2010).

65 Chung Y-I, Kim S-K, Lee Y-K *et al.* Efficient revascularization by VEGF administration via heparin-functionalized nanoparticle–fibrin complex. *J. Control. Release* 143(3), 282–289 (2010).

66 Chiappini C, De Rosa E, Martinez JO *et al.* Biodegradable silicon nanoneedles delivering nucleic acids intracellularly induce localized *in vivo* neovascularization. *Nat. Mater.* 14(5), 532–539 (2015).

•• **Codelivery of DNA and siRNA in silicon nanoneedles with high loading efficiency results in neovascularization and improved blood perfusion in a mouse model.**

67 Webber MJ, Tongers J, Newcomb CJ *et al.* Supramolecular nanostructures that mimic VEGF as a strategy for ischemic tissue repair. *Proc. Natl Acad. Sci. USA* 108(33), 13438–13443 (2011).

68 Rittchen S, Boyd A, Burns A *et al.* Myelin repair *in vivo* is increased by targeting oligodendrocyte precursor cells with nanoparticles encapsulating leukaemia inhibitory factor (LIF). *Biomaterials* 56, 78–85 (2015).

69 Savers S. FDA Guidance on Nanotechnology DOCUMENT: guidance for industry considering whether an FDA-regulated product involves the application of nanotechnology. *Biotechnol. Law Rep.* 30(5), 571–572 (2011).

•• **Describes the US FDA's position on the applications of nanotechnology, and suggests attention to safety, effectiveness, public health impact and regulatory status of nanotechnology-based products.**

70 Etheridge ML, Campbell SA, Erdman AG, Haynes CL, Wolf SM, Mccullough J. The big picture on nanomedicine: the state of investigational and approved nanomedicine products. *Nanomedicine* 9(1), 1–14 (2013).

71 Sinha R, Menon P, Chakranarayan S. Vitoss synthetic cancellous bone. *Med. J. Armed Forces India* 65(2), 173 (2009).

72 Witten CM. Summary Vitoss® Scaffold Synthetic Cancellous Bone Void Filler. (FDA Document, FDA) (2003). www.accessdata.fda.gov/cdrh_docs/pdf3/k032409.pdf

73 Lin C. Summary Ostim® Bone Grafting Material. (FDA Document, FDA, Rockville) (2004). www.accessdata.fda.gov/cdrh_docs/pdf3/K030052.pdf

74 Witten CM. Summary NanOssTM Bone Void Filler. (FDA Document, FDA) (2005). www.accessdata.fda.gov/cdrh_docs/pdf5/K050025.pdf

75 Henschke A. *Nanoscale: Issues and Perspectives for the Nano Century*. Cameron N, Mitchell ME (Eds). John Wiley & Sons, NJ, USA (2009).

76 Lin CS. Summary BoneGen-TR (FDA Document, FDA). (2006). www.accessdata.fda.gov/cdrh_docs/pdf6/K060285.pdf

77 Melkerso MN. Summary EquivaBone Osteoinductive Bone Graft Substitute. (FDA Document, FDA) (2009). www.accessdata.fda.gov/cdrh_docs/pdf9/K090855.pdf

78 Watson AD. Summary Beta-bsm Injectable Bone Substitute Material. (FDA Document, FDA) (2010). www.accessdata.fda.gov/cdrh_docs/pdf10/K102812.pdf

79 Watson AD. Summary NanoGen. (FDA Document, FDA). (2011). www.accessdata.fda.gov/cdrh_docs/pdf10/K102208.pdf

80 Melkerson Mark N. Summary Intervertebral body fusion device. (FDA Document, FDA). *Silver Spring* (2014). www.nanovisinc.com

81 Witten CM. Summary NB3D (nanOss Bioactive 3D) Bone Void Filler. (FDA Document, FDA) (2014). www.accessdata.fda.gov/cdrh_docs/pdf13/K132050.pdf

82 Verma S, Domb AJ, Kumar N. Nanomaterials for regenerative medicine. *Nanomedicine* 6(1), 157–181 (2011).

83 Shi J, Votruba AR, Farokhzad OC, Langer R. Nanotechnology in drug delivery and tissue engineering: from discovery to applications. *Nano Lett.* 10(9), 3223–3230 (2010).

Advanced nanobiomaterial strategies for the development of organized tissue engineering constructs

Nanobiomaterials, a field at the interface of biomaterials and nanotechnologies, when applied to tissue engineering applications, are usually perceived to resemble the cell microenvironment components or as a material strategy to instruct cells and alter cell behaviors. Therefore, they provide a clear understanding of the relationship between nanotechnologies and resulting cellular responses. This review will cover recent advances in nanobiomaterial research for applications in tissue engineering. In particular, recent developments in nanofibrous scaffolds, nanobiomaterial composites, hydrogel systems, laser-fabricated nanostructures and cell-based bioprinting methods to produce scaffolds with nanofeatures for tissue engineering are discussed. As in native niches of cells, where nanofeatures are constantly interacting and influencing cellular behavior, new generations of scaffolds will need to have these features to enable more desirable engineered tissues. Moving forward, tissue engineering will also have to address the issues of complexity and organization in tissues and organs.

KEYWORDS: bioprinting ■ hydrogel ■ laser biofabrication ■ nanobiomaterial ■ nanofiber

Jia An[1], Chee Kai Chua[1], Ting Yu[1], Huaqiong Li[2] & Lay Poh Tan*[2]

[1]Division of Systems & Engineering Management, School of Mechanical & Aerospace Engineering, Nanyang Technological University, Singapore
[2]Division of Materials Technology, School of Materials Science & Engineering, Nanyang Technological University, Singapore
**Author for correspondence: lptan@ntu.edu.sg*

Tissue engineering and regenerative medicine are promising new therapies to meet the global challenge of tissue/organ shortage [1]. However, the philosophy of tissue engineering and regenerative medicine varies considerably with the expertise of individual investigators, some use a biodegradable scaffold while others do not [2]. Currently, the speed of vascularization for implanted engineered tissues is generally low, and viable tissues that can be created, either *in vitro* or *in vivo*, are limited to structurally thin and relatively simple tissues such as skin, cartilage and bladder. Moreover, it is not unusual for the mechanical properties of engineered tissues to be inferior to their native counterparts. It is generally believed that the overall characteristics of an engineered tissue must result from its unique composition and organization of microstructures, such as the organization of cells and extracellular matrices, and that the problem of vascularization and inferiority are likely to be due to the microscale materials and structures within the tissue. Therefore, engineering extracellular matrices and promoting rapid formation of the cellular microenvironment is essential for advancing current tissue engineering and regenerative medicine. The building blocks of extracellular matrices are primarily nano- and micro-scale biomaterials that are dynamically synthesized, organized, remodeled and eliminated by cells. Their temporary presence in tissues usually allows direct physical contact with cell surface receptors, initiating an intracellular cascade of chemical reactions that eventually lead to various phenotypic behaviors such as adhesion, spreading, migration, DNA and protein synthesis, proliferation, senescence, apoptosis, orientation, and alignment. These nano- and micro-scale biomaterials mediate the microenvironment and cellular responses. Correct utilization of these materials can potentially unclock the code of cellular language and instruct cells to release their veiled potential for tissue repair and organ reconstruction.

Nanobiomaterials, at the interface of biomaterials and nanotechnology, refer to a special class of biomaterials with constituent or surface sizes less than 100 nm [3]. Their fine structure allows direct mechanical interactions with cell surface receptors and cellular components, and hence manipulation of cells to serve intended diagnostic or therapeutic purposes. Particularly when applied to tissue engineering and regenerative medicine, nanobiomaterials are usually perceived as microenvironment-like substances in which rich extracellular matrices and various cell types, including stem cells, reside. Nanobiomaterials, when applied to tissue engineering, are usually perceived as having a close resemblance to the microenvironment where cells reside. Through their interaction with cells, nanomaterials act as a means of providing instructive signals to the internal architecture of a cell.

There have been a number of attempts to engineer 3D tissues, but little progress has been made

Future Medicine part of fsg

on engineering 3D organized tissues (FIGURE 1). It is generally believed that the third dimension of an engineered tissue can not exist alone for a long period of time if there is no order being created at the nano- or micro-scale within the tissue. Therefore, it is of paramount importance to acquire further knowledge of nanobiomaterials in order to bridge the gap between biomaterials and nanotechnology, and to reveal their full potential for tissue engineering and regenerative medicine. This review discusses some recent progress on nanobiomaterial strategies in the field of tissue engineering and regenerative medicine, focusing on those with the potential for developing 3D organized tissue engineering constructs.

3D nanofibrous scaffolds & nanocomposites

Nanomaterials are widely utilized in tissue engineering and regenerative medicine because they are able to mimic compositions [4], topographies [5] and architectures [6] of human tissues, and may offer enhanced or new properties to artificial constructs [7]. They have been fabricated into various basic structural units, such as nanoparticles, nanocrystals, nanofibers and nanofilms, to fulfil the specific requirements of biological substitutes that repair or replace malfunctioning tissues [8]. Nanofibrous scaffolds, especially 3D scaffolds, have attracted considerable attention in tissue regeneration in recent years, mainly due to their structural similarity to native extracellular matrix, applicability to a wide range of materials, and readily tunable fiber size and spatial arrangement [9]. To date, nanofibrous scaffolds have been applied in research and regeneration of various tissues (e.g., skin [10,11], vascular [12], bone [13,14], cartilage [15], bladder [16], neural [17,18] and cardiac tissues [19]) *in vitro* and, more significantly, *in vivo*. 2D mats and 3D cotton-like balls are the two typical configurations used for nanofibrous scaffolds. In a recent study, Hsiao *et al.* fabricated an aligned 2D conductive nanofibrous mesh with poly(lactic-*co*-glycolic acid) and polyaniline to induce elongated and aligned rat cardiomyocyte clusters with synchronous cell beating [20]. However, 2D mats are less favorable unless the orientation or functionality of nanofibers is of great importance [21,22]. 2D mats, especially those that are electrospun, usually have a flat topography and tightly packed fibers that restrict cell infiltration to the superficial layers of the scaffolds and cellular integration with host tissue after implantation. Cell sheet technology transforms 2D nanofibrous mats into 3D functional tissues by stacking individual 2D confluent cell sheets recovered from thermoresponsive culture substrates [23,24]. In this manner, it extends the

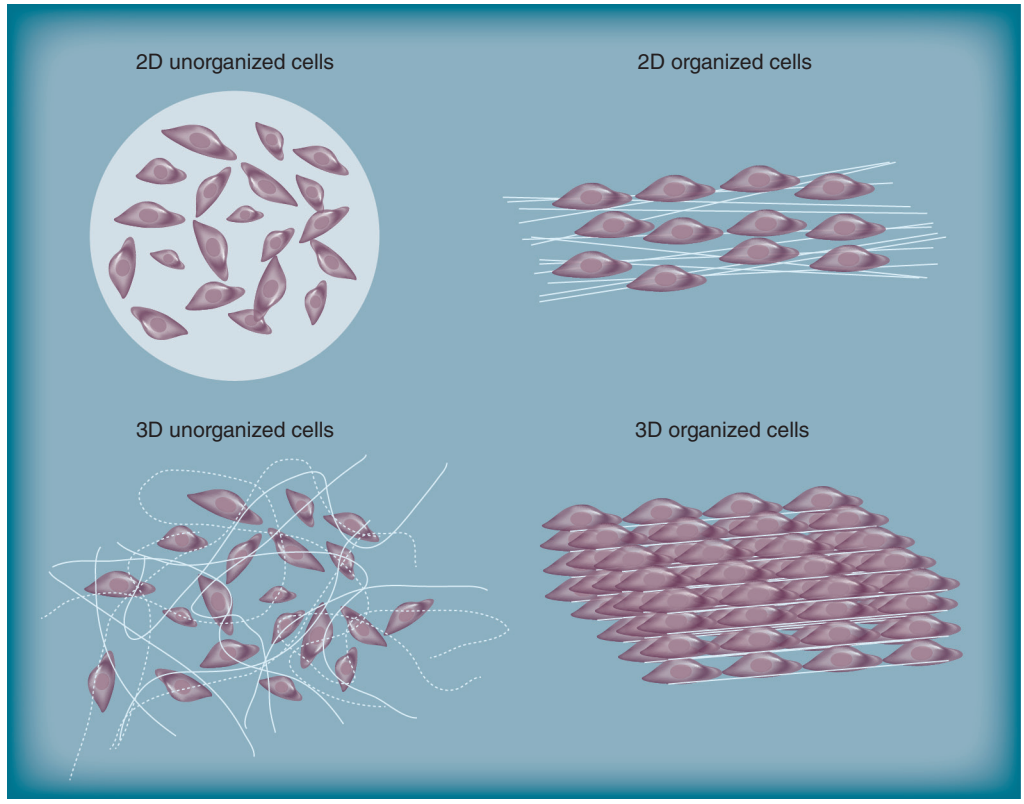

Figure 1. Organization of cells in engineered tissues.

application of 2D mats into producing implantable 3D tissues [25], but its potential will not be fully exploited until good nutrient transportation is achieved in thick cell stacks. Therefore, 3D nanofibrous scaffolds with proper pore size and interconnectivity are highly desirable to enable satisfactory cell infiltration and nutrient diffusion. Electrospinning is the most commonly used technique to fabricate 3D nanofibrous scaffolds with uniform morphology and stability; some are coupled with micrometer-sized framework [26,27] and some are directly electrospun [28,29]. Blakeney *et al.* devised a novel electrospinning collector that is an array of metal probes radially arranged in a spherical foam dish to harvest cotton ball-like poly(ε-caprolactone) scaffolds between the metal probes in mid-air (FIGURE 2). The resulting poly(ε-caprolactone) scaffolds were highly porous and cell infiltration was significantly improved [28]. In another study, Bonino *et al.* reported that 3D alginate nanofiber mats can be electrospun via charge repulsions from negatively charged ions dissociated by the carboxylic acid groups of alginate [29]. In addition to the methods mentioned above, a number of post-electrospinning techniques, such as polymer/salt leaching and laser/UV irradiation, are harnessed to improve the porosity of as-spun scaffolds [30]. Moreover, surface functionalization of electrospun fibers and drug encapsulation with nanofibers can further tailor the nanofibrous scaffolds to improve their performance, for example, by facilitating cell adhesion, spreading and growth, and controlled release of drugs [31].

In order to enhance certain properties or create new functionalities, multicomponent materials may be used to fabricate scaffolds [32]. On top of functional polymers such as electrically conductive polymers, hydroxyapatite, metal nanoparticles and carbon nanomaterials (e.g., fullerenes, carbon nanotubes and graphene) are often incorporated into polymeric matrix to fabricate nanocomposites for applications of tissue engineering and regenerative medicine. Hydroxyapatite, a biocompatible ceramic material mainly used in bone tissue engineering, is capable of resembling bone minerals in morphology and composition [33] and, thus, is extensively employed as part of nanocomposites in bone tissue engineering [34,35]. Electrically conductive materials are usually doped into a polymeric matrix to make conductive fibers/films for stimulating neurons and, hence, neural tissue repair [21]. In a recent study, aligned carbon nanotubes, rolled-up graphene sheets with excellent mechanical and electrical properties, were coated with para-toluene sulfonic acid-doped polypyrrole to form a novel nanostructured conductive platform, in which carbon nanotubes provided the topography and para-toluene sulfonic acid-doped polypyrrole provided the biocompatibility. It has been reported that the rate of differentiation and cell division of primary myoblasts cultivated on the conductive nanocomposite films can be controlled by electrical stimulation [36]. However, the potential toxicity of carbon nanomaterials has always been emphasized [37,38] and, although many *in vitro* experiments have demonstrated that they are nontoxic, the scientific community has to be fully convinced before any significant clinical applications can be realized [39,40]. Metals possess unique physical, chemical and biological properties when downsized to the nanometer scale compared with their macroscopic states. For instance, silver nanoparticles have been used for antibacterial applications. Agarwal *et al.* precisely controlled the loading of silver nanoparticles in thin polymeric films to allow antimicrobial activity without inducing cytotoxicity in mammalian cells [41]. Similar to carbon nanomaterials, the potential risk of metal nanoparticles should be fully understood and controlled before they are utilized in clinical applications.

Hydrogels

Hydrogels consist of a network of crosslinked polymer chains with the ability to absorb large amounts of water without disintegrating. This makes hydrogels unique and attractive as nanobiomaterials for tissue engineering and drug delivery applications. Hydrogels, including thermoresponsive and pH-sensitive gels, have

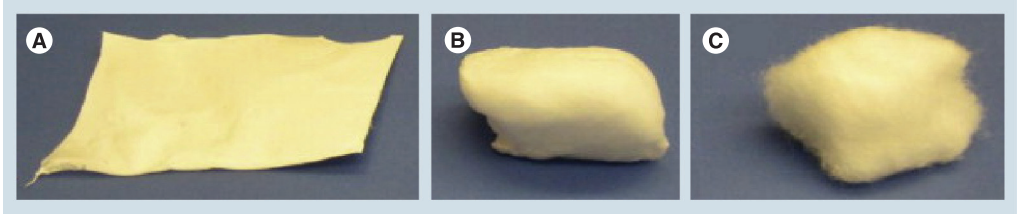

Figure 2. Electrospun nanofibrous scaffolds. (A) 2D nanofibrous scaffolds and **(B & C)** 3D nanofibrous scaffolds.

been researched extensively. Some of the more recent advancement in hydrogels for engineering 3D organized tissues will be reviewed. TABLE 1 shows desired properties of a hydrogel scaffold for 3D organized tissues and currently available strategies to achieve them.

In recent years, bioresponsive hydrogels have progressed substantially, bringing the engineering of a 3D organized tissue a step closer. One of these developments is spatially bioactive hydrogen. In work by Zhu *et al.*, a biomimetic hydrogel scaffold with controlled spatial organization of nanobiomaterials, such as cell-adhesive ligands, was developed [42]. Cyclic Arg–Gly–Asp peptides were first attached in the middle of poly(ethylene glycol) diacrylate (PEGDA) chains and hydrogel formation was initiated via photopolymerization. The authors showed that cyclic Arg–Gly–Asp–PEGDA hydrogels could facilitate endothelial cell adhesion and spreading, and exhibited significantly higher endothelial cell proliferation compared with linear Arg–Gly–Asp-modified hydrogels at low peptide incorporations. Incorporation of cell-adhesive ligands and controlling ligand density and spatial organization is an initial but critical step for hydrogels to be three-dimensionally responsive to cellular adhesions. Stimulation of microenvironmental factors, such as electrical signals, has also been shown to be important because some tissues, such as muscles, require electrical stimuli to function. Mawad *et al.* developed a single component, conducting hydrogel by covalently crosslinking a poly(3-thiopheneacetic acid) hydrogel with 1.1′-carbonyldiimidazole [43]. In addition to swelling ratios up to 850%, the hydrogels were shown to be electroactive and conductive at physiological pH. In terms of cellular responses, fibroblast and myoblast cells were able to adhere and proliferate well on the hydrogel substrate.

One of the common problems with hydrogels is their poor mechanical properties. To enhance the mechanical properties of hydrogels, incorporating nanobiomaterials into hydrogels could be a possible solution. As shown by Kai *et al.*, incorporation of poly(ε-caprolactone) nanofibers into gelatin hydrogel resulted in the increase of the Young's modulus of the composite hydrogels from 3.29 to 20.3 kPa. [44]. Wu *et al.* studied the photocrosslinking of poly(ethylene oxide)–poly(propylene oxide)–poly(ethylene oxide) triblock copolymer diacrylates (Pluronic® F127 diacrylate; BASF, Ludwigshafen, Germany) in the presence of the silicate nanoparticle Laponite® (Rockwood Additives, TX, USA) and the resulting hydrogels had high elongations and improved toughness [45]. Chang *et al.* developed PEGDA/Laponite nanocomposite hydrogels, and the incorporation of Laponite nanoparticles significantly enhanced both the compressive and tensile properties of PEGDA hydrogels [46]. The authors also demonstrated that their nanocomposite hydrogels were able to support 3D cell culture. In addition to mechanical advantages, incorporation of nanobiomaterials also offers bioactive advantages. Azami *et al.* prepared a gelatin–amorphous calcium phosphate nanocomposite scaffold that has a three-dimensionally interconnected porous microstructure. After incubation in simulated body fluid solution at 37°C for 5 days, the mineral phase of the scaffold was transformed into nanocrystalline hydroxyapatite [47]. Sowmyaa *et al.* reported a chitin hydrogel scaffold lyophilized with bioactive glass ceramic nanoparticles, which was found to have enhanced porosity, swelling, bioactivity and degradation [48]. Moreover, the composite scaffolds were nontoxic to human osteoblasts and suitable for periodontal bone defects. Sudheesh Kumar *et al.* developed chitin/nanosilver composite scaffolds that were effective against *Escherichia coli* and *Staphylococcus aureus* [49].

Spatially controlled release of growth factors is a desired property of a tissue engineering scaffold, and this may be conveniently realized after the invention of nanogels. Nanogels are a special type of hydrogel in which hydrogel nanoparticles or nanogels (<100 nm) are either chemically or physically crosslinked by polymer chains to form a 3D network [50]. Owing to their nanometer size, nanogels are more effective at stably trapping bioactive compounds inside their network and respond more rapidly to microenvironmental factors such as temperature and pH. Therefore, nanogels are important for spatially controlled release of growth factors within a scaffold. FIGURE 3 shows a schematic of the preparation of a cholesterol-bearing pullulan nanogel-crosslinking hydrogel to deliver BMP-2 [51]. Hayashi *et al.* examined the efficiency of

Table 1. Nanobiomaterial strategies for enhancing the properties of hydrogels.

Desired properties of hydrogel scaffold	Nanobiomaterial strategies
Bioresponsiveness	Nanoscale ligands
Mechanical strength	Nanocomposites
Controlled release of growth factors	Nanogels
Properties of native proteins	Self-assembled peptides

nanogels to deliver BMP-2 *in vivo* for bone defect repair. Despite a single implantation with low amounts of BMP, vigorous osteoblastic activation and new bone formation were evident [51]. Kamolratanakul *et al.* went further by delivering a combination of a selective EP4 receptor agonist and a low dose of BMP-2 in a nanogel-based disc scaffold, and observed efficient activation of bone cells and effective regeneration of bone tissues [52]. In another study, Bencherif *et al.* hybridized nanogels to hyaluronic acid by mixing them under physiological conditions (pH = 7.4; 37°C), and created a nanostructured hyaluronic acid hydrogel scaffold with a porous 3D uniform distribution of nanogels [53].

In addition to the aforementioned properties, there is considerable interest in developing self-assembled peptide nanostructure to

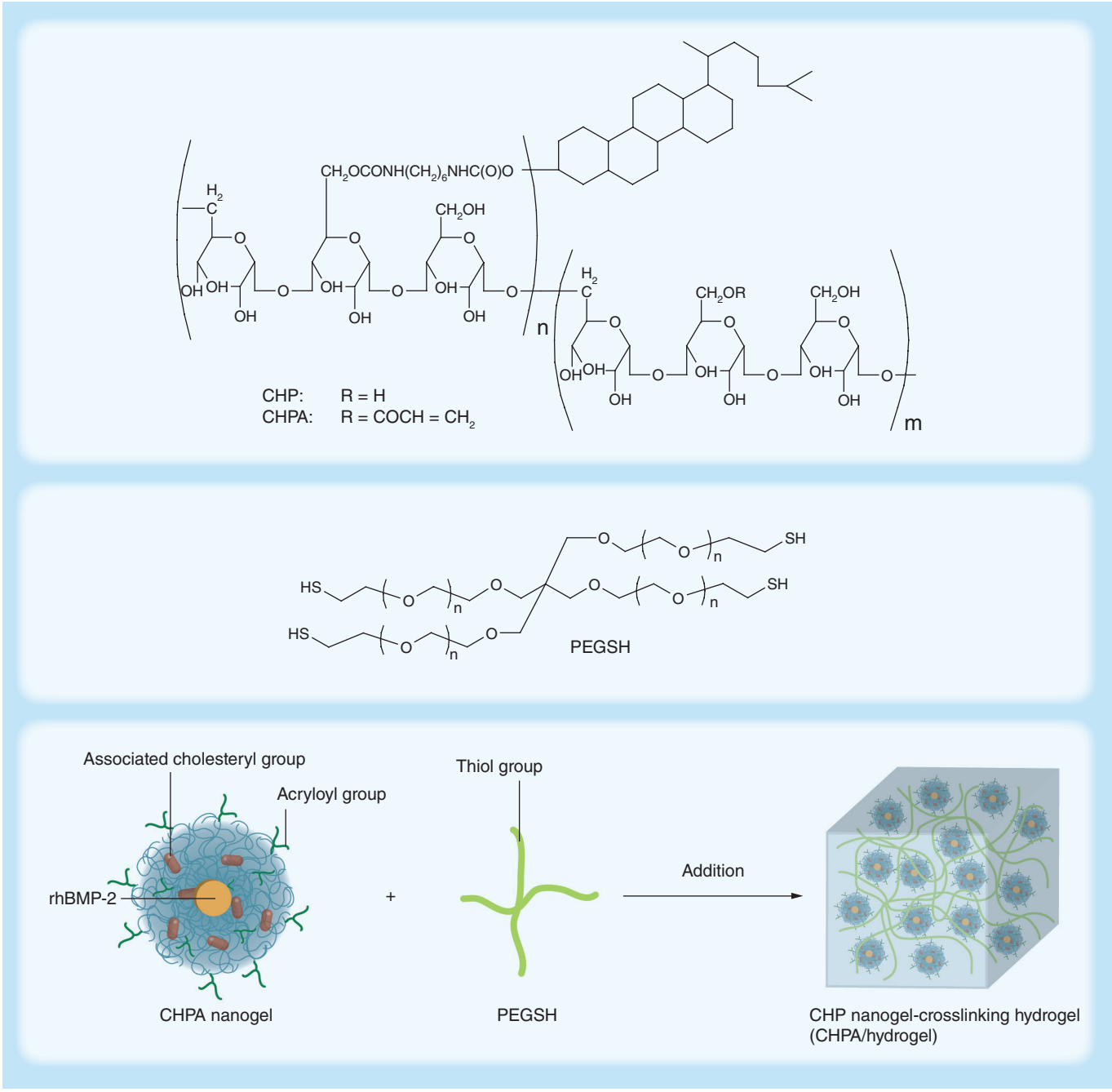

Figure 3. Acryloyl group-modified cholesterol-bearing pullulan nanogel-crosslinking hydrogel containing BMP-2 growth factor.
CHP: Cholesterol-bearing pullulan; CHPA: Acryloyl group-modified CHP; PEGSH: Thiol group-modified poly(ethylene glycol); rhBMP-2: Recominant human BMP-2.
Reproduced with permission from [51].

mimic the creation process of native proteins. O'Leary *et al.* designed a peptide sequence (Pro–Lys–Gly)$_4$(Pro–Hyp–Gly)$_4$(Asp–Hyp–Gly)$_4$ that can form a stable triple helix and replicates the self-assembly of collagen through all steps. The resulting nanofibres can form a hydrogel that is degraded by collagenase at a similar rate to that of natural collagen [54]. The ability to design and synthesize peptides with characteristics that are similar to their native counterparts can offer significant advantages in the control and manipulation of scaffold properties.

Laser-fabricated 3D nanostructures

Laser technology is able to generate fine features, such as ridges, grooves and standing rods, among others, on a 2D surface, and it has shown remarkable influence on various cell behaviors, including cell attachment, orientation, proliferation and differentiation [55–58]. Most, if not all, of these studies are conducted on a 2D platform on which the properties of the nanoscale features such as spacing, width and height of ridges are constructed. The laser forms different features that mimic natural extracellular matrix features, which causes the cells to interact with the artificial construct as they would *in vivo*. Using laser-machined biomaterials with nanoscale features may potentially help us to gain a better understanding of biological mechanisms, such as cell adhesion on a biomaterial surface, which is mainly directed by molecular interactions at the nanoscale [59]. These studies contribute greatly to the fundamental understanding of the role of nanoscale topography, but have little correlation with the role of spatial nanostructures on 3D tissues. One of the main reasons this area is not progressing as fast is the lack of adequate methods to generate 3D nanostructures. Additive manufacturing technology is a group of techniques that could possibly address this, as it is able to fabricate 3D constructs based on a layer-by-layer principle.

The advantages of using the additive manufacturing approach to fabricate 3D nanostructures is the controllability of process parameters and, hence, the resulting consistency of scaffold properties. Selective laser sintering [60,61] and stereolithography [62,63] are two widely used techniques to fabricate 3D scaffolds for tissue engineering and regenerative medicine applications. However, distinct disadvantages limit their application. One of the obvious drawbacks is resolution, or rather the lack of resolution, as selective laser sintering and stereolithography can only fabricate precisely controlled scaffolds with geometrical dimensions ranging from tens to hundreds of micrometers, which is too large to mimic the unique microenvironment of natural tissues *in vivo* with submicron and nanoscale cues. With recent advancements in 3D laser nonlinear lithographic technology [64,65], multiphoton polymerization, especially two-photon polymerization (2PP), has been applied to create 3D nanostructures in a scaffold [66,67]. This technique has achieved the highest resolution (with feature sizes as small as 100 nm and even a size of 30 nm has been reported [68]) so far in the family of additive manufacturing technology. The resolution of 2PP is adjustable, which conveniences the tuning and thus saves fabrication time [69].

2PP has been applied to a wide range of materials, from synthetic polymers (e.g., biodegradable triblock copolymer [70] and nonbiodegradable polymer Ormocer®, VOCO GmbH, Cuxhaven, Germany [71,72]) to proteins (e.g., fibrinogen [73,74], collagen type I and bovine serum albumin [75]), and even different metal-based sol–gel composites (e.g., Zr- or Ti-based composites [76,77]). Among these widely used materials, PEGDA, with its biocompatibility and nonfouling properties, is a very good candidate for tissue engineering scaffold fabrication after 2PP treatment [78,79]. Figure 4 shows a scaffold fabricated by 2PP. The 3D structure is sophisticated and intricate, with a minimum feature size of 200 nm. Many PEGDA-based 3D scaffolds formed by 2PP have already been evaluated for their biocompatibility, including cytotoxicity [78], cell adhesion and cell viability [80]. There is a report that even showed a promising approach through the integration 2PP and laser-induced forward transfer to fabricate arbitrary PEGDA-based 3D structures with predesigned submicron features [81]. This technique offers a new approach to achieve 3D multicellular tissue constructs with an engineered extracellular matrix. It is also very interesting to notice that 2PP can crosslink natural polymers, potentially allowing the exploration of proteins and DNA as templates for the construction of 3D scaffolds [82]. In their report, the authors found that the laser formed protein scaffolds with precisely designed topographies that could be used as a new bioelectronics platform for monitoring and simulating biological processes [82], such as cellular signal transduction and neuronal networking [83,84]. Many properties of 2PP-generated 3D structures can also contribute to medical devices, such as small prosthetics [71,85,86]. Ovsianikov and coworkers manufactured total ossicular replacement prostheses out of Ormocer [87]. 2PP is a very important process in the synthesis

of Ormocer. The flexibility of 2PP makes the dimension of total ossicular replacement prostheses adjustable, which would be conducive to regenerative medicine applications.

Although 2PP has already proven to be a powerful technique for tissue engineering scaffold fabrication, there are still some drawbacks that limit its widespread usage. One of these factors is production time. Recently, several advanced methods have been explored to improve the throughput of laser fabrication. In a study by Zhang and Chen, the combination of 2PP and nanoimprinting was presented as an effective way to produce nanofeatures in the hydrogel in a massively parallel way [67]. Another trial utilized multibeam fabrication to shorten the 2PP process [88].

Using a laser to create nanofeatures is proven for 2D structures, but for 3D structures there remain challenges. However, there are emerging techniques that have shown feasibility, and as science and technology advances, this is probably going to be a very viable method.

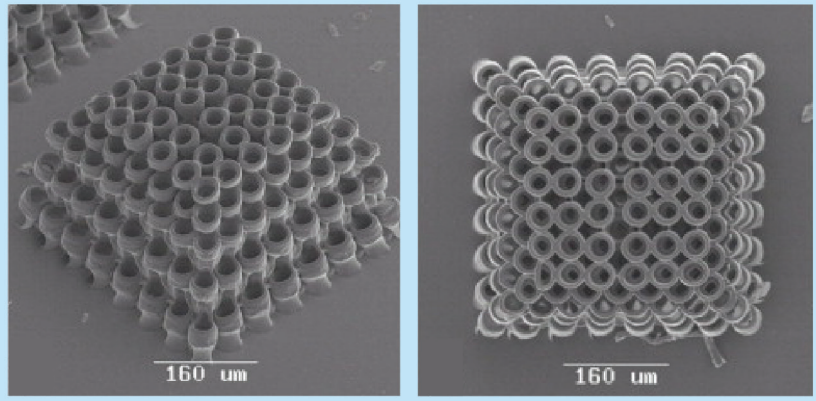

Figure 4. Highly organized 3D scaffold structure fabricated by two-photon polymerization. The minimum feature size is 200 nm.
Reproduced with permission from [78].

Bioprinting of cells

All the techniques discussed above involve the fabrication of advanced scaffolds to support cells.

In this section, another method to directly manipulate the microstructure of tissues at the cellular level to build up the organization of tissue, without the use of scaffolds, will be discussed. Bioprinting refers to a special additive manufacturing technology that processes cells and biological materials into the physical counterpart of a predefined 3D computer model. From the point of view of manufacturing, the resolution of the bioprinting process is below 100 µm, although not within the nanoscale. However, from the point of view of interactions between cells and materials, the scale of bioprinted biologics ranges from micrometers (e.g., cells) to nanometers (e.g., focal adhesion complexes and integrins).

In one study of bioprinting, cells were first prepared in the form of tissue spheroids in a robotic system [89], and then mixed with a hydrogel and printed one-by-one in a defined layout, such as a ring or a branched structure. Over time, these printed tissue spheroids can fuse and integrate to form tissue with an ordered organization [90]. In another method, a laser was used to assist printing of controlled 2D cellular patterns, such as the Olympic symbol shown in FIGURE 5, in a high-resolution and high-speed manner at the microscale [91]. Recently, multiple cell types have been separately mixed with crosslinkers ($CaCl_2$) and loaded into separate ink cartridges for inkjet printing [92]. The multiple-cell pie configuration shown in FIGURE 6A consists of human amniotic fluid-derived stem cells, canine smooth muscle cells and bovine aortic endothelial cells. All printed cell types maintained their viability and normal physiological functions within

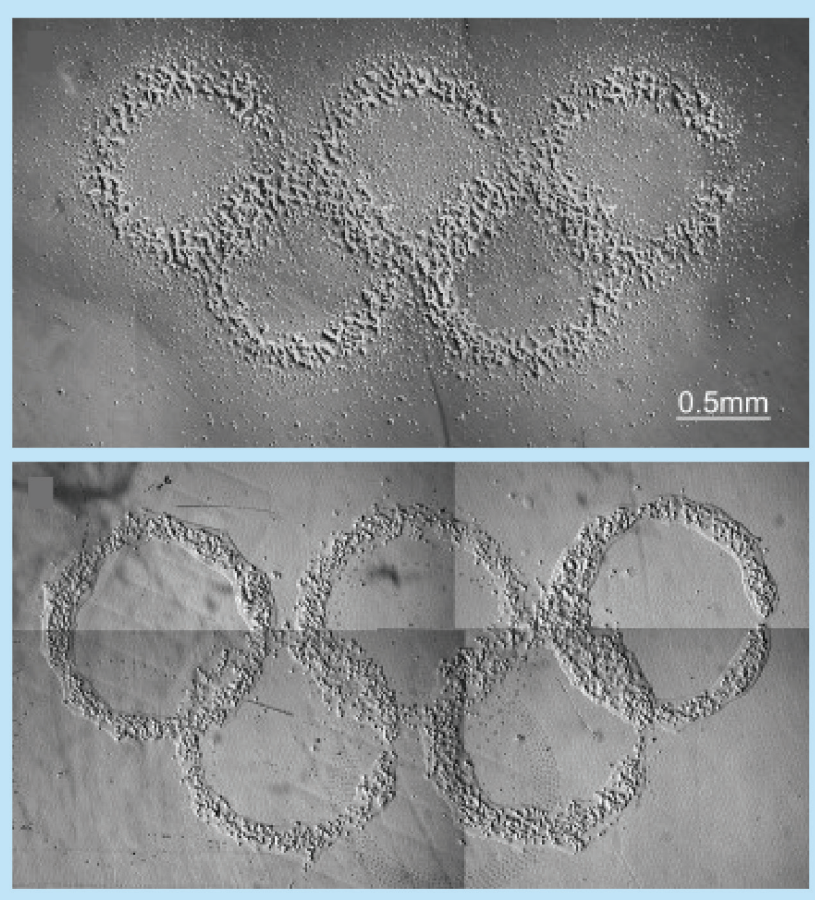

Figure 5. Laser-assisted bioprinting of 2D cellular patterns.
Reproduced with permission from [91].

the hybrid constructs (FIGURE 6B). The bioprinted constructs were adequately vascularized *in vivo* and matured into functional tissues (FIGURE 6C).

Bioprinting of cells is very much in its infancy and there are practical challenges ahead. Currently, one practical limitation of bioprinting is the weak mechanical strength of bioprinted hydrogels [93]. Development of a bioprintable hydrogel that is suitable for the bioprinting process, as well as for cell encapsulation and viability, is critical. Censi *et al.* evaluated the suitability of a biodegradable, photopolymerizable and thermosensitive A–B–A triblock copolymer hydrogel, in which poly(*N*-(2-hydroxypropyl) methacrylamide lactate) forms A blocks and hydrophilic poly(ethylene glycol) forms B blocks [94]. They demonstrated layer-by-layer deposition of hydrogel fibers, forming stable 3D constructs with high viability of encapsulated chondrocytes. Another practical challenge in bioprinting is the concurrent printing and culture of mixed multiple cell types. There are a few approaches that may be considered for fabricating a construct with mixed multiple cell types; for example, deposition of multiple types of cells through multiple nozzles or deposition of tissue spheroids that already contain a mixture of multiple cell types. Nonetheless, these approaches only address the issue of how to aggregate multiple types of cells; at the fundamental level, how to concurrently culture and grow multiple cell types is still unclear. Norotte *et al.* reported the use of various vascular cell types, including smooth muscle cells and fibroblasts, for bioprinting [2], but these cell types were not seeded at precise locations within a single scaffold and post-printing culture has not involved in their study. Although Schuurman *et al.* claimed to be able to bioprint a hybrid tissue construct [95], their actual work is limited to multiple cells of a single cell type, not multiple cell types. Currently, there is also considerable interest in the strategy of *in situ* bioprinting [96], in which the mixture of cells and hydrogels are directly deposited onto defect areas such as skin burns. This strategy could potentially eliminate the problems of *in vitro* bioprinting and provide rapid tissue repair, thus promising to be a new therapy in the future.

Conclusion

In conclusion, various nanobiomaterial strategies have shown some promising aspects in terms of

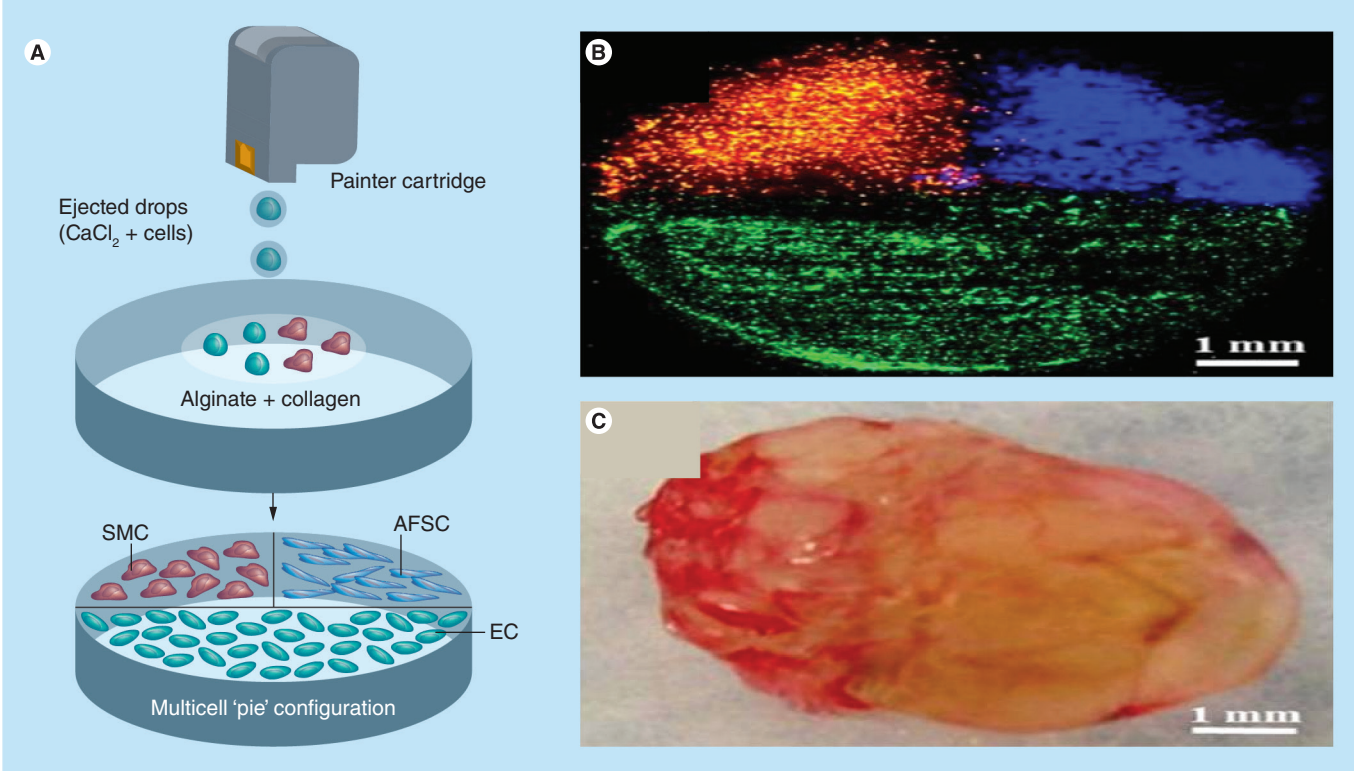

Figure 6. Inkjet bioprinting of 3D tissue engineering constructs consisting of multiple cell types. (A–C) The multiple-cell pie configuration. **(B)** All cell types maintained their viability and normal physiological functions within the hybrid constructs, **(C)** which were adequately vascularized *in vivo* and matured into functional tissues.
AFSC: Amniotic fluid-derived stem cell; EC: Endothelial cell; SMC: Smooth muscle cell.
Reproduced with permission from [92].

Table 2. Nanobiomaterial strategies for developing 3D organized tissue engineering constructs.

Nanobiomaterial strategy	Advantages	Disadvantages	Organization
Nanofibrous scaffolds and nanocomposites	Established 2D nanofeature guidance on cells and 3D bulk nanofibrous constructs available	Unorganized 3D bulk structure, inadequate pore size and strength, and poor consistency	Unorganized
Hydrogels	Ability to hold water and swell, resemble living tissues and ease of applicability	Inadequate bioactivity and strength, and poor internal structure	Less organized cell–scaffold constructs
Laser fabrication	Rapid fabrication and highly controllable organized 3D scaffolds available	Few biomaterials can easily be laser processed	Organized scaffold structure
Bioprinting	Established principle of layer-by-layer printing of preliminary cell/tissue constructs	Inadequate hydrogel strength, and great biological challenge of printing and culture of heterogeneous cells	Organized cells and tissue structure

Nanobiomaterial strategies are listed in ascending degree of organization.

addressing the issue of complexity and organization in tissues and organs, but no single strategy is a complete solution to this challenge. TABLE 2 summarizes the advantages and disadvantages of each and suggests that, based on the degree of organization of current 3D constructs, the bioprinting strategy is now closer to these aims than other strategies, and could be a viable approach in the future.

Future perspective

Various recent nanobiomaterial strategies have been reviewed in this paper to highlight their potential for engineering 3D organized tissue. Moving forward, tissue engineering and regenerative medicine will have to address the issues of complexity and organization in tissues and organs. Future work should include manipulation of nanobiomaterials toward the engineering of a more ordered 3D tissue microstructure, and should reveal more on the relationship between tissue microstructure and the resulting characteristics of an engineered tissue.

Financial & competing interests disclosure

The authors have no relevant affiliations or financial involvement with any organization or entity with a financial interest in or financial conflict with the subject matter or materials discussed in the manuscript. This includes employment, consultancies, honoraria, stock ownership or options, expert testimony, grants or patents received or pending, or royalties.

No writing assistance was utilized in the production of this manuscript.

Executive summary

- Tissue engineering and regenerative medicine are restricted by a limited tissue thickness and poorly organized tissue microstructures.
- In recent years, research on nanobiomaterials for tissue engineering and regenerative medicine applications has emerged, due to their ability to direct cell behaviors toward desired tissue outcomes.
- Recent progresses in 3D nanofibrous scaffolds and nanocomposites, hydrogels, laser-fabricated nano- and micro-structures, and bioprinting enable the possibility of developing 3D organized tissue engineering constructs to address the issues of complexity and organization in tissues and organs.
- Bioprinting is a very promising approach for developing 3D organized tissue constructs, but it is still in its infancy and is yet to overcome the practical challenges to truly deliver a printed functional tissue or organ.

References

Papers of special note have been highlighted as:
- ▪ of interest
- ▪▪ of considerable interest

1 Langer R, Vacanti JP. Tissue engineering. *Science* 260(5110), 920–926 (1993).

2 Norotte C, Marga FS, Niklason LE, Forgacs G. Scaffold-free vascular tissue engineering using bioprinting. *Biomaterials* 30(30), 5910–5917 (2009).

3 Yang L, Zhang L, Webster TJ. Nanobiomaterials: state of the art and future trends. *Adv. Eng. Mater.* 13(6), B197–B217 (2011).

4 Wei GB, Ma PX. Structure and properties of nano-hydroxyapatite/polymer composite scaffolds for bone tissue engineering. *Biomaterials* 25(19), 4749–4757 (2004).

5 Xu CY, Inai R, Kotaki M, Ramakrishna S. Aligned biodegradable nanotibrous structure: a potential scaffold for blood vessel engineering. *Biomaterials* 25(5), 877–886 (2004).

6 Teo WE, Liao S, Chan C, Ramakrishna S. Fabrication and characterization of hierarchically organized nanoparticle-reinforced nanofibrous composite scaffolds. *Acta Biomater.* 7(1), 193–202 (2011).

7 Li YQ, Yu T, Yang TY, Zheng LX, Liao K. Bio-inspired nacre-like composite films based on graphene with superior mechanical,

electrical, and biocompatible properties. *Adv. Mater.* 24(25), 3426–3431 (2012).

8 Zhang LJ, Webster TJ. Nanotechnology and nanomaterials: promises for improved tissue regeneration. *Nano Today* 4(1), 66–80 (2009).

9 Pham QP, Sharma U, Mikos AG. Electrospinning of polymeric nanofibers for tissue engineering applications: a review. *Tissue Eng.* 12(5), 1197–1211 (2006).

10 Kumbar SG, Nukavarapu SP, James R, Nair LS, Laurencin CT. Electrospun poly(lactic acid-*co*-glycolic acid) scaffolds for skin tissue engineering. *Biomaterials* 29(30), 4100–4107 (2008).

11 Zhu XL, Cui WG, Li XH, Jin Y. Electrospun fibrous mats with high porosity as potential scaffolds for skin tissue engineering. *Biomacromolecules* 9(7), 1795–1801 (2008).

12 Hu JA, Sun XA, Ma HY *et al.* Porous nanofibrous PLLA scaffolds for vascular tissue engineering. *Biomaterials* 31(31), 7971–7977 (2010).

13 Zhang YZ, Venugopal JR, El-Turki A *et al.* Electrospun biomimetic nanocomposite nanofibers of hydroxyapatite/chitosan for bone tissue engineering. *Biomaterials* 29(32), 4314–4322 (2008).

14 Gupta D, Venugopal J, Mitra S, Giri Dev VR, Ramakrishna S. Nanostructured biocomposite substrates by electrospinning and electrospraying for the mineralization of osteoblasts. *Biomaterials* 30(11), 2085–2094 (2009).

15 Tortelli F, Cancedda R. Three-dimensional cultures of osteogenic and chondrogenic cells: a tissue engineering approach to mimic bone and cartilage *in vitro*. *Eur. Cell. Mater.* 17, 1–14 (2009).

16 Tian, H, Bharadwaj S, Liu Y *et al.* Myogenic differentiation of human bone marrow mesenchymal stem cells on a 3D nano fibrous scaffold for bladder tissue engineering. *Biomaterials* 31(5), 870–877 (2010).

17 Ghasemi-Mobarakeh L, Prabhakaran MP, Morshed M, Nasr-Esfahani MH, Ramakrishna S. Electrospun poly(epsilon-caprolactone)/gelatin nanofibrous scaffolds for nerve tissue engineering. *Biomaterials* 29(34), 4532–4539 (2008).

18 Prabhakaran MP, Venugopal JR, Ramakrishna S. Mesenchymal stem cell differentiation to neuronal cells on electrospun nanofibrous substrates for nerve tissue engineering. *Biomaterials* 30(28), 4996–5003 (2009).

19 Orlova Y, Magome N, Liu L, Chen Y, Agladze K. Electrospun nanofibers as a tool for architecture control in engineered cardiac tissue. *Biomaterials* 32(24), 5615–5624 (2011).

20 Hsiao CW, Bai MY, Chang Y *et al.* Electrical coupling of isolated cardiomyocyte clusters grown on aligned conductive nanofibrous meshes for their synchronized beating. *Biomaterials* 34, 1063–1072 (2013).

21 Ghasemi-Mobarakeh L, Prabhakaran MP, Morshed M, Nasr-Esfahani MH, Ramakrishna S. Electrical stimulation of nerve cells using conductive nanofibrous scaffolds for nerve tissue engineering. *Tissue Eng. Part A* 15(11), 3605–3619 (2009).

22 Wang CY, Zhang KH, Fan CY *et al.* Aligned natural–synthetic polyblend nanofibers for peripheral nerve regeneration. *Acta Biomater.* 7(2), 634–643 (2011).

23 Matsuda N, Shimizu T, Yamato M, Okano T. Tissue engineering based on cell sheet technology. *Adv. Mater.* 19(20), 3089–3099 (2007).

24 Masuda S, Shimizu T, Yamato M, Okano T. Cell sheet engineering for heart tissue repair. *Adv. Drug Deliv. Rev.* 60(2), 277–285 (2008).

25 Haraguchi Y, Shimizu T, Sasagawa T *et al.* Fabrication of functional three-dimensional tissues by stacking cell sheets *in vitro*. *Nat. Protoc.* 7(5), 850–858 (2012).

26 Moroni L, Schotel R, Hamann D, de Wijn JR, van Blitterswijk CA. 3D fiber-deposited electrospun integrated scaffolds enhance cartilage tissue formation. *Adv. Func. Mater.* 18(1), 53–60 (2008).

27 Kim G, Son J, Park S, Kim W. Hybrid process for fabricating 3D Hierarchical Scaffolds combining rapid prototyping and electrospinning. *Macromol. Rapid Commun.* 29(19), 1577–1581 (2008).

28 Blakeney BA, Tambralli A, Anderson JM *et al.* Cell infiltration and growth in a low density, uncompressed three-dimensional electrospun nanofibrous scaffold. *Biomaterials* 32(6), 1583–1590 (2011).

▪ **First article to report a truly 3D nanofibrous scaffold in bulk form.**

29 Bonino CA, Efimenko K, Jeong SI *et al.* Three-dimensional electrospun alginate nanofiber mats via tailored charge repulsions. *Small* 8(12), 1928–1936 (2012).

30 Zhong S, Zhang Y, Lim CT. Fabrication of large pores in electrospun nanofibrous scaffolds for cellular infiltration: a review. *Tissue Eng. Part B Rev.* 18(2), 77–87 (2012).

31 Jang JH, Castano O, Kim HW. Electrospun materials as potential platforms for bone tissue engineering. *Adv. Drug Deliv. Rev.* 61(12), 1065–1083 (2009).

32 Armentano I, Dottori M, Fortunati E, Mattioli S, Kenny JM. Biodegradable polymer matrix nanocomposites for tissue engineering: a review. *Polym. Degrad. Stabil.* 95(11), 2126–2146 (2010).

33 Langelaan ML, Boonen KJ, Rosaria-Chak KY, van der Schaft DW, Post MJ, Baaijens FP. Advanced maturation by electrical stimulation: differences in response between C2C12 and primary muscle progenitor cells. *J. Tissue Eng. Regen. Med.* 5(7), 529–539 (2011).

34 Venugopal JR, Low S, Choon AT, Kumar AB, Ramakrishna S. Nanobioengineered electrospun composite nanofibers and osteoblasts for bone regeneration. *Artif. Organs* 32(5), 388–397 (2008).

35 Huang YX, Ren J, Chen C, Ren TB, Zhou XY. Preparation and properties of poly(lactide-*co*-glycolide) (PLGA)/nano-hydroxyapatite (NHA) scaffolds by thermally induced phase separation and rabbit MSCs culture on scaffolds. *J. Biomater. Appl.* 22(5), 409–432 (2008).

36 Quigley AF, Razal JM, Kita M. Electrical stimulation of myoblast proliferation and differentiation on aligned nanostructured conductive polymer platforms. *Adv. Healthc. Mater.* 1, 801–808 (2012).

37 Firme CP 3rd, Bandaru PR. Toxicity issues in the application of carbon nanotubes to biological systems. *Nanomedicine* 6(2), 245–256 (2010).

38 Oberdorster G. Safety assessment for nanotechnology and nanomedicine: concepts of nanotoxicology. *J. Intern. Med.* 267(1), 89–105 (2010).

39 Agarwal, S XZ, Zhou, F. Ye *et al.* Interfacing live cells with nanocarbon substrates. *Langmuir* 26(4), 2244–2247 (2010).

40 Agarwal S, Zhou X, Ye F *et al.* Cellular behavior of human mesenchymal stem cells cultured on single-walled carbon nanotube film. *Carbon* 48(4), 1095–1104 (2010).

41 Agarwal A, Weis TL, Schurr MJ *et al.* Surfaces modified with nanometer-thick silver-impregnated polymeric films that kill bacteria but support growth of mammalian cells. *Biomaterials* 31(4), 680–690 (2010).

42 Zhu J, Tang C, Kottke-Marchant K, Marchant RE. Design and synthesis of biomimetic hydrogel scaffolds with controlled organization of cyclic RGD peptides. *Bioconjug. Chem.* 20(2), 333–339 (2009).

43 Mawad D, Stewart E, Officer DL *et al.* A single component conducting polymer hydrogel as a scaffold for tissue engineering. *Adv. Func. Mater.* 22(13), 2692–2699 (2012).

44 Kai D, Prabhakaran MP, Stahl B, Eblenkamp M, Wintermantel E, Ramakrishna S. Mechanical properties and *in vitro* behavior of nanofiberhydrogel composites for tissue engineering applications. *Nanotechnology* 23(9), 095705 (2012).

45 Wu CJ, Gaharwar AK, Chan BK, Schmidt G. Mechanically tough Pluronic F127/Laponite

nanocomposite hydrogels from covalently and physically cross-linked networks. *Macromolecules* 44(20), 8215–8224 (2011).

46 Chang CW, Van Spreeuwel A, Zhang C, Varghese S. PEG/clay nanocomposite hydrogel: a mechanically robust tissue engineering scaffold. *Soft Matter* 6(20), 5157–5164 (2010).

47 Azami M, Moosavifar MJ, Baheiraei N, Moztarzadeh F, Ai J. Preparation of a biomimetic nanocomposite scaffold for bone tissue engineering via mineralization of gelatin hydrogel and study of mineral transformation in simulated body fluid. *J. Biomed. Mater. Res. A* 100(5), 1347–1356 (2012).

48 Sowmyaa S, Sudheesh Kumar PT, Chennazhia KP, Naira SV, Tamurab H, Jayakumara R. Biocompatible β–chitin hydrogel/nanobioactive glass ceramic nanocomposite scaffolds for periodontal bone regeneration. *Trends Biomater. Artif. Organs* 25(1), 1–11 (2011).

49 Sudheesh Kumar PT, Abhilash S, Manzoor K *et al.* Preparation and characterization of novel β-chitin/nanosilver composite scaffolds for wound dressing applications. *Carbohyd. Polym.* 80(3), 761–767 (2010).

50 Sasaki Y, Akiyoshi K. Nanogel engineering for new nanobiomaterials: from chaperoning engineering to biomedical applications. *Chem. Rec.* 10(6), 366–376 (2010).

51 Hayashi C, Hasegawa U, Saita Y *et al.* Osteoblastic bone formation is induced by using nanogel-crosslinking hydrogel as novel scaffold for bone growth factor. *J. Cell. Physiol.* 220(1), 1–7 (2009).

52 Kamolratanakul P, Hayata T, Ezura Y *et al.* Nanogel-based scaffold delivery of prostaglandin E(2) receptor-specific agonist in combination with a low dose of growth factor heals critical-size bone defects in mice. *Arthritis Rheum.* 63(4), 1021–1033 (2011).

53 Bencherif SA, Washburn NR, Matyjaszewski K. Synthesis by AGET ATRP of degradable nanogel precursors for in situ formation of nanostructured hyaluronic acid hydrogel. *Biomacromolecules* 10(9), 2499–2507 (2009).

54 O'Leary LE, Fallas JA, Bakota EL, Kang MK, Hartgerink JD. Multi-hierarchical self-assembly of a collagen mimetic peptide from triple helix to nanofibre and hydrogel. *Nat. Chem.* 3(10), 821–828 (2011).

55 Stratakis E, Ranella A, Farsari M, Fotakis C. Laser-based micro/nanoengineering for biological applications. *Prog. Quant. Electron.* 33(5), 127–163 (2009).

56 Wang X, Ohlin CA, Lu Q, Hu J. Cell directional migration and oriented division on three-dimensional laser-induced periodic surface structures on polystyrene. *Biomaterials* 29(13), 2049–2059 (2008).

57 Rebollar E, Frischauf I, Olbrich M *et al.* Proliferation of aligned mammalian cells on laser-nanostructured polystyrene. *Biomaterials* 29(12), 1796–1806 (2008).

58 Mirzadeh H, Moghadam EV, Mivehchi H. Laser-modified nanostructures of PET films and cell behavior. *J. Biomed. Mater. Res. A* 98(1), 63–71 (2011).

59 Seidlits SK, Lee JY, Schmidt CE. Nanostructured scaffolds for neural applications. *Nanomedicine (Lond.)* 3(2), 183–199 (2008).

60 Tan KH, Chua CK, Leong KF *et al.* Scaffold development using selective laser sintering of polyetheretherketone–hydroxyapatite biocomposite blends. *Biomaterials* 24(18), 3115–3123 (2003).

61 Leong KF, , Cheah CM, Chua CK. Solid freeform fabrication of three-dimensional scaffolds for engineering replacement tissues and organs. *Biomaterials* 24(13), 2363–2378 (2003).

62 Cooke MN, Fisher JP, Dean D, Rimnac C, Mikos AG. Use of stereolithography to manufacture critical-sized 3D biodegradable scaffolds for bone ingrowth. *J. Biomed. Mater. Res. Part B Appl. Biomater.* 64(2), 65–69 (2003).

63 Lee KW, Wang S, Fox BC, Ritman EL, Yaszemski MJ, Lu L. Poly(propylene fumarate) bone tissue engineering scaffold fabrication using stereolithography: effects of resin formulations and laser parameters. *Biomacromolecules* 8(4), 1077–1084 (2007).

64 Cumpston BH, Ananthavel SP, Barlow S *et al.* Two-photon polymerization initiators for three-dimensional optical data storage and microfabrication. *Nature* 398(6722), 51–54 (1999).

65 Jun Y, Nagpal P, Norris DJ. Thermally stable organic–inorganic hybrid photoresists for fabrication of photonic band gap structures with direct laser writing. *Adv. Mater.* 20(3), 606–610 (2008).

66 Li L, Fourkas JT. Multiphoton polymerization. *Mater. Today* 10(6), 30–37 (2007).

67 Zhang W, Chen S. Femtosecond laser nanofabrication of hydrogel biomaterial. *MRS Bull.* 36(12), 1028–1033 (2011).

68 Juodkazis S, Mizeikis V, Seet KK, Miwa M, Misawa H. Two-photon lithography of nanorods in SU-8 photoresist. *Nanotechnology* 16(6), 846 (2005).

69 Gittard SD, Miller PR, Boehm RD *et al.* Multiphoton microscopy of transdermal quantum dot delivery using two photon polymerization-fabricated polymer microneedles. *Faraday Discuss.* 149(0), 171–185 (2011).

70 Claeyssens F, Hasan EA, Gaidukeviciute A *et al.* Three-dimensional biodegradable structures fabricated by two-photon polymerization. *Langmuir* 25(5), 3219–3223 (2009).

71 Doraiswamy A, Jin C, Narayan RJ *et al.* Two photon induced polymerization of organic–inorganic hybrid biomaterials for microstructured medical devices. *Acta Biomater.* 2(3), 267–275 (2006).

72 Gittard SD, Narayan RJ. Laser direct writing of micro- and nano-scale medical devices. *Expert Rev. Med. Dev.* 7(3), 343–356 (2010).

73 Pitts JD, Campagnola PJ, Epling GA, Goodman SL. Submicron multiphoton free-form fabrication of proteins and polymers: studies of reaction efficiencies and applications in sustained release. *Macromolecules* 33(5), 1514–1523 (2000).

74 Anastasia K, Shaun G, Sabrina S *et al.* Fabrication of fibrin scaffolds with controlled microscale architecture by a two-photon polymerization–micromolding technique. *Biofabrication* 4(1), 015001 (2012).

75 Pitts JD, Howell AR, Taboada R *et al.* New photoactivators for multiphoton excited three-dimensional submicron cross-linking of proteins: bovine serum albumin and type 1 collagen. *Photochem. Photobiol.* 76(2), 135–144 (2002).

76 Ovsianikov A, Viertl J, Chichkov B *et al.* Ultra-low shrinkage hybrid photosensitive material for two-photon polymerization microfabrication. *ACS Nano* 2(11), 2257–2262 (2008).

77 Sakellari I, Gaidukeviciute A, Giakoumaki A *et al.* Two-photon polymerization of titanium-containing sol–gel composites for three-dimensional structure fabrication. *Appl. Phys. A* 100(2), 359–364 (2010).

78 Ovsianikov A, Malinauskas M, Schlie S *et al.* Three-dimensional laser micro- and nano-structuring of acrylated poly(ethylene glycol) materials and evaluation of their cytoxicity for tissue engineering applications. *Acta Biomater.* 7(3), 967–974 (2011).

▪ **Reports the nano- and micro-scale structuring of poly(ethylene glycol) diacrylate materials by two-photon polymerization.**

79 Gittard SD, Ovsianikov A, Akar H *et al.* Two photon polymerization-micromolding of polyethylene glycol-gentamicin sulfate microneedles. *Adv. Eng. Mater.* 12(4), B77–B82 (2010).

80 Weiß T, Schade R, Laube T *et al.* Two-photon polymerization of biocompatible photopolymers for microstructured 3D biointerfaces. *Adv. Eng. Mater.* 13(9), B264–B273 (2011).

81 Ovsianikov A, Gruene M, Pflaum M *et al.* Laser printing of cells into 3D scaffolds. *Biofabrication* 2(1), 014104 (2010).

82 Hill RT, Lyon JL, Allen R, Stevenson KJ, Shear JB. Microfabrication of three-dimensional bioelectronic architectures. *J. Am. Chem. Soc.* 127(30), 10707–10711 (2005).

83 Kaehr B, Ertaş N, Nielson R *et al.* Direct-write fabrication of functional protein matrixes using a low-cost Q-switched laser. *Anal. Chem.* 78(9), 3198–3202 (2006).

84 Lyon JL, Hill RT, Shear JB, Stevenson KJ. Direct electrochemical and spectroscopic assessment of heme integrity in multiphoton photo-cross-linked cytochrome C structures. *Anal. Chem.* 79(6), 2303–2311 (2007).

85 Ovsianikov A, Schlie S, Ngezahayo A, Haverich A, Chichkov BN. Two-photon polymerization technique for microfabrication of CAD-designed 3D scaffolds from commercially available photosensitive materials. *J. Tissue Eng. Regen. Med.* 1(6), 443–449 (2007).

86 Anastasia K, Sabrina S, Elena F *et al.* Microreplication of laser-fabricated surface and three-dimensional structures. *J. Opt.* 12(12), 124009 (2010).

87 Ovsianikov A, Chichkov B, Adunka O *et al.* Rapid prototyping of ossicular replacement prostheses. *Appl. Surf. Sci.* 253(15), 6603–6607 (2007).

88 Obata K, Koch J, Hinze U, Chichkov BN. Multi-focus two-photon polymerization technique based on individually controlled phase modulation. *Opt. Express.* 18(16), 17193–17200 (2010).

89 Mehesz AN, Brown J, Hajdu Z *et al.* Scalable robotic biofabrication of tissue spheroids. *Biofabrication* 3(2), 025002 (2011).

90 Mironov V, Trusk T, Kasyanov V *et al.* Biofabrication: a 21st century manufacturing paradigm. *Biofabrication* 1(2), 022001 (2009).

91 Guillotin B, Souquet A, Catros S *et al.* Laser assisted bioprinting of engineered tissue with high cell density and microscale organization. *Biomaterials* 31(28), 7250–7256 (2010).

▪▪ **First study to report a high-resolution and high-speed method for deposition and organization of cells.**

92 Xu T, Zhao W, Zhu JM *et al.* Complex heterogeneous tissue constructs containing multiple cell types prepared by inkjet printing technology. *Biomaterials* 34(1), 130–139 (2013).

▪▪ **First study to report bioprinting of a heterogeneous tissue construct and conduct both an *in vitro* and *in vivo* evaluation.**

93 Billiet T, Vandenhaute M, Schelfhout J, Van Vlierberghe S, Dubruel P. A review of trends and limitations in hydrogel-rapid prototyping for tissue engineering. *Biomaterials* 33(26), 6020–6041 (2012).

94 Censi R, Schuurman W, Malda J *et al.* A printable photopolymerizable thermosensitive p(HPMAm-lactate)–PEG hydrogel for tissue engineering. *Adv. Func. Mater.* 21(10), 1833–1842 (2011).

95 Schuurman W, Khristov V, Pot MW *et al.* Bioprinting of hybrid tissue constructs with tailorable mechanical properties. *Biofabrication* 3(2), 021001 (2011).

96 Binder KW, Zhao W, Aboushwareb T *et al.* *In situ* bioprinting of the skin for burns. *J. Am. Coll. Surg.* 211(3), S76 (2010).

Research Article

For reprint orders, please contact: reprints@futuremedicine.com

Journal of
3D Printing in Medicine

3D segmentation of intervertebral discs: from concept to the fabrication of patient-specific scaffolds

T Oner[1,2], IF Cengiz[1,2], M Pitikakis[3], L Cesario[3], P Parascandolo[3], L Vosilla[3], G Viano[3], JM Oliveira[1,2], RL Reis[1,2] & J Silva-Correia[*,1,2]

[1]3B's Research Group – Biomaterials, Biodegradables and Biomimetics, University of Minho, Headquarters of the European Institute of Excellence on Tissue Engineering and Regenerative Medicine, Avepark – Parque de Ciência e Tecnologia, Zona Industrial da Gandra, 4805–017 Barco GMR, Portugal

[2]ICVS/3B's – PT Government Associated Laboratory, Braga, Portugal

[3]Softeco Sismat Srl, Genova, Italy

*Author for correspondence:
Tel.: +351 253 510 931
Fax: +351 253 510 909
joana.correia@dep.uminho.pt

Aim: To develop a methodology for producing patient-specific scaffolds that mimic the annulus fibrosus (AF) of the human intervertebral disc by means of combining MRI and 3D bioprinting. **Methods:** In order to obtain the AF 3D model from patient's volumetric MRI dataset, the RheumaSCORE segmentation software was used. Polycaprolactone scaffolds with three different internal architectures were fabricated by 3D bioprinting, and characterized by microcomputed tomography. **Results:** The demonstrated methodology of a geometry reconstruction pipeline enabled us to successfully obtain an accurate AF model and 3D print patient-specific scaffolds with different internal architectures. **Conclusion:** The results guide us toward patient-specific intervertebral disc tissue engineering as demonstrated by a way of manufacturing personalized scaffolds using patient's MRI data.

First draft submitted: 3 November 2016; Accepted for publication: 26 January 2017; Published online: 3 March 2017

Keywords: 3D bioprinting • intervertebral disc • MRI segmentation • patient-specific approach • rapid prototyping • reverse engineering • tissue engineering

The intervertebral disc (IVD) is a fibrocartilaginous tissue composed of a gelatinous nucleus pulposus (NP) surrounded by the cartilaginous endplates (CEP) on the upper and lower surfaces, and the annulus fibrosus (AF) laterally. The discs are the pivot point of the spine, allowing different direction movements, such as bending, rotating and twisting [1]. The primary functions of IVD are to absorb and distribute unbalanced forces through the ligaments and muscles, and to transmit spine loads that can occur as a result of motions between the vertebral bodies [2,3]. However, the IVD cannot fulfill its normal functions in pathologic conditions such as the loss of disc height (first stage of disc degeneration), endplate-driven or annulus-driven degeneration and disc herniation [4,5], and due to other reasons like physical fitness, bone mass index and smoking [6].

The current treatments mainly include the use of drugs to address the symptoms such as pain and the surgical treatments (i.e., discectomy, spinal fusion, artificial IVD replacement and the use of allogeneic or autogeneic tissues). They neither relieve pain permanently nor regenerate the tissue. Given the reported reherniation, promoted degeneration in adjacent IVDs and the changed biomechanics of the spine after the surgical treatments, it is correct to say that the clinical need has not yet been completely met [7–10]; there is a need for regenerative strategies. Tissue engineering (TE) advanced treatment strategies have promised the restoration of NP [11–15] or AF [16–19] and total disc replacement [19–21]. In simple words, in the desired TE scenario, new tissue formation occurs by extracellular matrix synthesis of implanted cells, while the biodegradable scaffold that carries and hosts the cells degrades over time. Current TE strategies consider that constructs need to have other properties besides mimicking the extracellular matrix (ECM) of the tissues to

Future Medicine part of fsg

be regenerated. The importance of developing patient-specific scaffolds is gaining a new impetus [22,23]. The need for having patient-specific IVD scaffolds is evident, given the fact that the size and shape of IVDs vary from patient to patient, and within a patient they vary within the position in the spine [1,24].

Herein, we demonstrate a step-by-step methodology to produce patient-specific scaffolds starting from the patient's MRI data. Moreover, the 3D model obtained by segmentation can also be used for the preparation and elaboration of 3D surgery planning and the assessment of its difficulties by simulating the operation before the surgical procedure [23,25].

3D reconstructions of anatomical structures are indispensable for medical diagnosis, visualization as well as 3D printing of patient-specific implants [22,26,27]. The process of 3D reconstruction of all the relevant tissues is based on the segmentation of medical imaging data. Existing image segmentation methods vary from manual slice-by-slice segmentation to fully automatic ones [28]. Attempts to fully automate the segmentation procedure are often unreliable or targeted on a limited set of specific tissues. On the other hand, interactive segmentation approaches can combine the efficiency, accuracy and repeatability of automatic methods with human expertise and quality assurance. RheumaSCORE [29], developed by Softeco Sismat S.r.l. [30], is a computer-aided diagnosis software tool that supports and assists the user in the diagnosis and the management of chronic diseases, such as rheumatoid arthritis. One of the features is that RheumaSCORE supports an interactive and real-time segmentation tool, based on a variation of the level-set algorithm for the segmentation and morphological identification of the tissues [22,31]. Other free or open source tools that can provide similar image segmentation functionality with RheumaSCORE include ITK-SNAP [32], 3D Slicer [33], GIST [34] and Analyze [35].

The level-set method [36] was employed in our previous work [22]. The level-set approach is a versatile method for the computation and analysis of the motion of an interface Γ, in two or three dimensions. It is based on the representation of a contour as the zero level set of a higher dimensional function, and formulation of the movement of the contour as the evolution of the level-set function. It is aimed to compute and analyze the subsequent motion of Γ under a velocity field $\vec{u}$. This velocity can depend on time, position, the geometry of the interface and/or external physics. The interface is captured as the zero level set of a smooth function $\varphi(x,t)$. The evolving contour/surface can be extracted from the zero level set $\Gamma(x,t) = [(x,t)|\ \varphi(x,t) = 0]$ with $\varphi:R^n \rightarrow R$. The motion function $Y(x,t)$ consists of a combination of two parts:

$$\frac{\partial \phi}{\partial t} = |\nabla \phi| \left[\alpha D(x) + (1-\alpha) \nabla \cdot \frac{\nabla \phi}{|\nabla \phi|} \right]$$

where D is a data part that forces the model toward desirable features in the input data; the part $\nabla\cdot(\nabla\varphi/|\nabla\varphi|)$ is the mean curvature of the surface, which forces the surface to have a smaller area; and $\alpha\varepsilon[0,1]$ is a free parameter that controls the degree of smoothness in the solution. There are several variants and extensions of the level-set method in the literature. One of them is the geodesic level-set method [37], which is used in the software. The distinctive characteristics of this method are that it focuses on a sparse field solver approach, and the speed function D (which acts as the principal 'force' that drives the segmentation) is the result of the combination of two terms: $D_{intensity}$ and D_{fuzzy}. The term $D_{intensity}$ is based on the input grayscale value of the voxel x, while the term D_{fuzzy} describes the affinity between contiguous voxels.

The present study is a part of the patient-specific IVD TE strategy that we envision, as depicted in Figure 1, that is, we aim to develop a standard methodology using MRI and computer-aided design combined with 3D printing for the fabrication of patient-specific IVD scaffolds from polycaprolactone (PCL) with different internal architectures. The PCL scaffolds were characterized by microcomputed tomography (μ-CT) to evaluate the effects of the internal architecture on the microstructure.

Materials & methods

MRI segmentation & 3D model reconstruction of the human IVD tissue

A 47-year-old male patient underwent an MRI scan in head-first supine position with the use of a 3.0-T scanner (Siemens MAGNETOM Spectra, Munich, Germany) using spin echo T2-weighted sequence. A Digital Imaging and Communication in Medicine (DICOM) dataset with a high spatial resolution was obtained, and the acquisition plane was sagittal. The DICOM dataset had 80 slices with a voxel size of 0.9 × 0.9 × 0.9 mm^3 and a slice thickness of 0.9 mm, with an echo time of 145 ms, repetition time of 1400 ms and an echo train length of 64.

The geometry reconstruction pipeline for generating the 3D IVD model consists of three main steps:

- Image segmentation – a proprietary software application called RheumaSCORE (v 0.1.16; Softeco Sismat S.r.l., Genova, Italy) was used for the segmentation of the MRI images. Exterior boundaries separate structures of interest and background, while interior boundaries separate anatomical areas which have different features, in other words, the

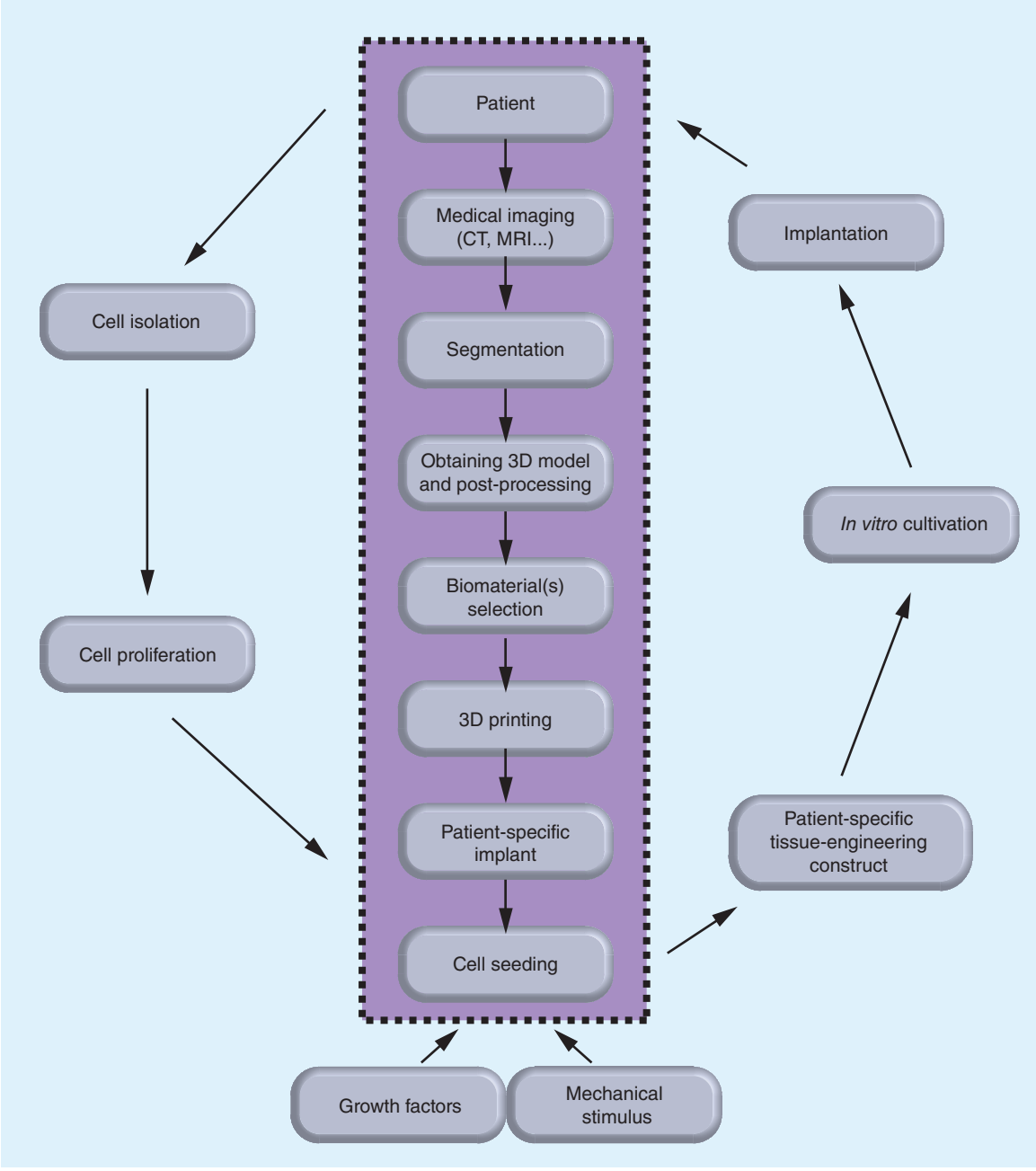

Figure 1. Representation of the envisioned patient-specific intervertebral disc tissue engineering strategy with the highlighted role of the present study in the center. The data obtained from medical imaging of the patient's intervertebral disc (IVD) are segmented and processed into a 3D model to be used in 3D printing the selected biomaterial(s) of a patient-specific IVD implant. Different types of biomaterials can be used for reproducing the annulus fibrosus and nucleus pulposus. The autologous cells are isolated from the patient, proliferated *in vitro* and introduced into patient-specific scaffold in the presence of growth factors and mechanical stimulus. The tissue engineered patient-specific construct cultured *in vitro* can be then implanted into the patient.

contact areas between the different tissues. The segmentation process is performed with an operator integration to benefit from the use of landmarks for the detection of exterior/interior borders of the contouring areas to separate CEP and AF.

- Manual corrections on the segmented images – some manual refinements were needed to improve the accuracy of the segmented images. The user interface of the tool allows manual error corrections after segmentation or during segmentation using the draw/erase mode.

- 3D reconstruction – from a given 3D scalar field of voxels, all boundary surfaces are to be computed. The 3D model reconstruction was obtained from the segmented images, and the 3D model was converted into a stereolithography format using the software, which includes this 3D model generation and conversion to stereolithography feature.

Fabrication of patient-specific IVD scaffolds

The 3D model of the IVD was isotropically resized to half size to be practical, and sliced into 0.167-mm-thick layers with the software provided by EnvisionTec GmbH (Germany). Using a fourth-generation 3D Bioplotter (EnvisionTec GmbH, Dearborn, Michigan, USA), three patient-specific IVD scaffolds were printed with three different internal architectures resulting from a layer-wise alternating strand directions either as 0°/90° (architecture A), 0°/60°/120° (architecture B) or 0°/45°/90°/135° (architecture C). In each layer, the strands were parallel to each other and 1 mm apart from each other. For printing the scaffolds, PCL (average M_n = 45,000) purchased from Sigma-Aldrich (MO, USA) was melted at 110°C in the cartridge of the 3D Bioplotter and extruded as strands through a 22G heated metal needle, at a speed of 5 mm/s and under the pressure of 5 bar.

μ-CT analysis

Three samples of each of the three architectures were scanned with a high-resolution desktop x-ray μ-CT system (SkyScan 1272; Bruker MicroCT, Kontich, Belgium) for the 3D morphometric analysis. The x-ray source voltage and current were set at 50 kV and 200 μA, respectively. About 800 projections with 10 μm of isotropic pixel size were acquired over a rotation range of 360° with a rotation step of 0.45°. The 2D cross-sectional images were reconstructed from the x-ray projections. On each 2D images, a grayscale threshold of 32–255 was applied, and a region of interest was defined to obtain a volume of interest dataset which was used for the 3D morphometric analysis performed by using the CT Analyser software (version 1.15.4.0) supplied by Bruker MicroCT.

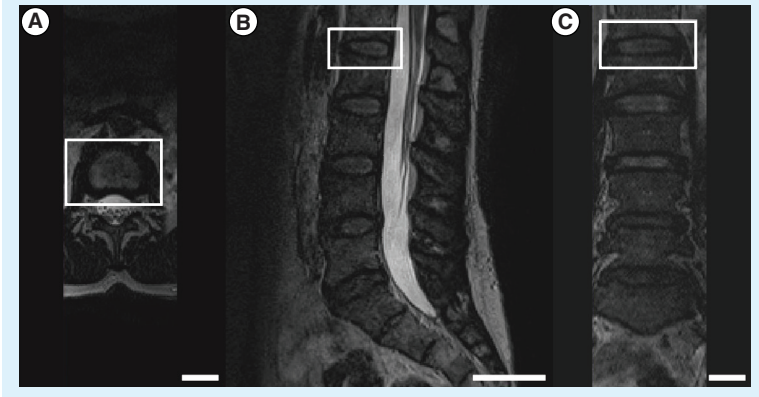

Figure 2. MRI images of the patient. Images taken from the **(A)** axial, **(B)** sagittal and **(C)** coronal planes. The L1–L2 intervertebral disc was indicated by the white rectangle (scale bars: 4 cm).

Statistical analysis

Statistical analysis was performed using SPSS® (IBM® SPSS® Statistics version 23.0; IBM, USA). One-way analysis of variance (ANOVA) tests were used to determine the statistically significant differences between the three different architectures in each structural property (i.e., mean pore size, porosity and interconnectivity). The level of significance used was set at $p < 0.05$ for a 95% CI.

Results & discussion

MRI segmentation & 3D human IVD model reconstruction

The DICOM dataset having 80 3D T2-weighted MRI images with a voxel size of 0.9 × 0.9 × 0.9 mm^3 was obtained for the segmentation of the L1–L2 IVD of the patient. Figure 2 shows the MRI images of the patient from different planes. In our work, we utilized the RheumaSCORE software which uses a variation of the level-set algorithm. CEP and AF have similar intensity on the 2D images; therefore, the landmarks were identified manually inside the interest region of the 2D images for the detection of exterior/interior borders of the contouring areas to distinguish CEP and AF. Also, with the use of the presegmentation tool of RheumaSCORE, that is, grayscale thresholding function, it was possible to segment the AF without the NP component of the IVD. From the final image segmentation, a 3D surface model was reconstructed with RheumaSCORE (Figure 3). A requirement for having high-quality 3D models is to have volumetric images with identical resolution in all dimensions, that is, isotropic. The DICOM images of the patient were almost isotropic and with high spatial resolution. For a precise segmentation, besides having a high spatial resolution, it is also necessary to obtain the accurate geometric structure of the IVD. Based on our work, an MRI with a smaller voxel size was possible to achieve. Nevertheless, a smaller voxel size may cause a high noise that dramatically affects the segmentation quality, and the final outcome can be worse. The high noise results from long acquisition time and involuntary movement of the spine of the patient during the MRI acquisition process.

In this study, T2-weighted MRI was used as medical image visualization and a semiautomatic

segmentation was performed for segmentation of the disc, as an alternative to manual and automatic segmentation. Since manual segmentation is a completely operator-dependent and time-consuming process, the manually drawing of the region of interest requires proper skills and adequate software tools with sophisticated graphical user interface [38]. On the other hand, semiautomatic segmentation has been proposed to minimize supervised operator needs of manual segmentation as well as to allow error correction during the segmentation process, unlike automatic segmentation.

Although we have used the acquired 3D IVD model to produce scaffold, the proposed model can be utilized for several other objectives including, but not limited to, finite element modeling [39]. In addition, the 3D models of the IVD and spine may be preferred over the 2D images by the surgeon for the presurgery planning.

In the last decade, level-set methods which have emerged for the segmentation of images [40], are based on a calculus of piecewise constant variational equations. Moreover, the method can represent contours with complex topology and allow any topological changes naturally. Experiments related to the segmentation of the IVDs were performed using the level-set algorithm, and the segmentation method was determined as a semiautomatic mode which uses a combination of supervised active contour segmentation and postprocessing carried out manually in the following slices. In MRI, hard and soft tissues can be roughly discriminated by characteristic scalar values, in other words, grayscale. Thus, they can be quickly computed as isosurfaces, that is, surfaces passing through voxels of the same scalar value. Typically, anatomical structures are in complex shape, and their curved boundary surfaces are essential to preserve. These boundary surfaces are represented by a set of triangles that are convenient to render using graphics hardware. However, CEP and AF have similar scalar values. Therefore, there is a need for some amount of user interaction. To address this issue, we are currently working to develop a methodology to fully automate the IVD segmentation process; this procedure will allow enhancing the accuracy and reproducibility of the segmentation while minimizing workload, user interaction and extensive postprocessing after the segmentation.

3D fabrication of patient-specific IVD scaffolds

The 3D patient-specific IVD model (Figure 4) was obtained by the segmentation of the MRI. The dataset was isotropically resized to half size and sliced into 25 layers possessing a thickness of 0.167 mm each (Figure 5A & B). Three distinct internal architectures were developed as shown in Figure 5C–E. The architectures of scaffolds A–C are composed of alternating layers of 0°/90°, 0°/60°/120° and 0°/45°/90°/135° strands, respectively. Figure 6 shows the 3D-printed patient-specific IVD scaffolds with different architectures. Herein, a methodology from MRI acquisition to the 3D-printed IVD scaffolds has been demonstrated to be the critical part of the envisioned patient-specific IVD TE strategy. PCL was selected as the biomaterial for the 3D printing because it is a biomaterial that gathers appropriate properties for rapid prototyping. Once the patient-specific IVD model is obtained, it is possible to tailor the scaffold architecture, as such three basic architectures were studied; and a higher number of different and more complex architectures can be designed.

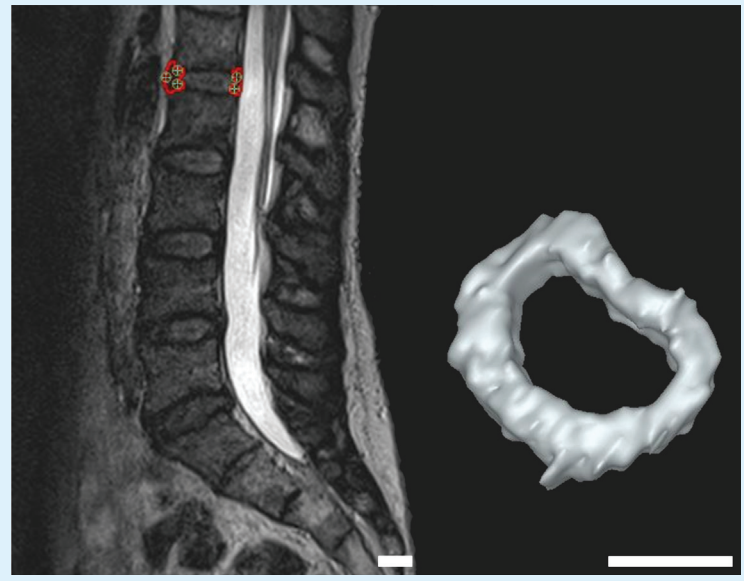

Figure 3. The segmentation process. Left: L1–L2 intervertebral disc of the patient. Right: the 3D model of the intervertebral disc after completing the segmentation (scale bars: 2 cm).

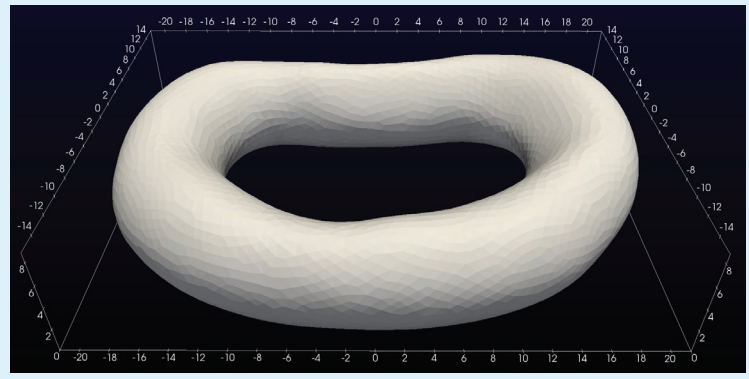

Figure 4. The final smoothed 3D model of the L1–L2 intervertebral disc of the patient. The numbers correspond to millimeter.

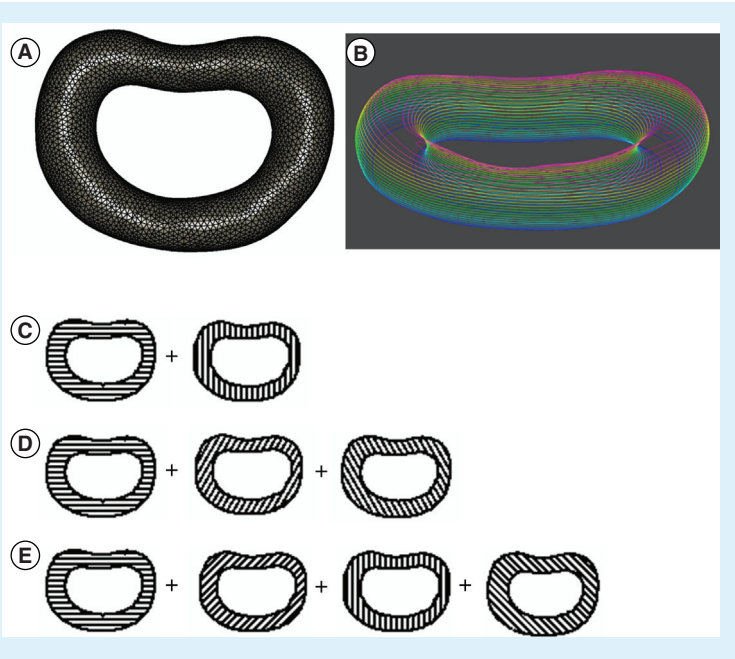

Figure 5. Patient-specific 3D intervertebral disc model, its layers, and the layer-wise alternating strand directions. (A) The wireframe 3D model of the intervertebral disc (IVD) of the patient; **(B)** the layers of the 3D IVD model after slicing of the 3D model into layers with colors changing from red to blue indicating the top and the bottom layer, respectively; the illustration of the alternating layers in the three architectures: architectures A–C with **(C)** 0°/90°, **(D)** 0°/60°/120° and **(E)** 0°/45°/90°/135° strand structures, respectively.

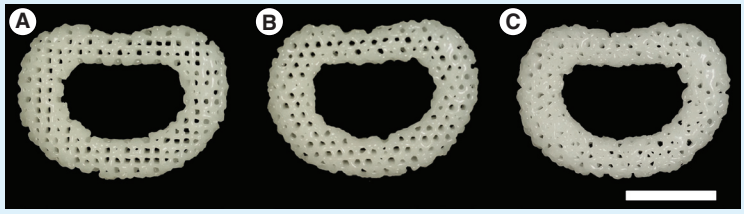

Figure 6. Photographs of the 3D printed intervertebral disc scaffolds with three different internal architectures. (A) Architecture A (0°/90° strand structure). **(B)** Architecture B (0°/60°/120° strand structure). **(C)** Architecture C (0°/45°/90°/135° strand structure) (scale bars: 1 cm).

We have demonstrated a step-by-step methodology to produce patient-specific scaffolds starting from the patient's MRI data. Moreover, the 3D model obtained through segmentation can also be used for the preparation and elaboration of 3D surgery planning and the assessment of its difficulties by simulating the operation before the surgical procedure [23,25]. With the aim of moving further with the knowledge arising from the present studies, the methodology herein demonstrated is currently being investigated for obtaining complex IVD TE implants by means of combining bio-inks (e.g., silk fibroin and methacrylated gellan gum hydrogels) and stem cells.

μ-CT analysis of the 3D-printed scaffolds

The structural and morphometric features of the 3D-fabricated samples with the three different architectures were analyzed by μ-CT. The 2D and 3D images are shown in Figure 7. The μ-CT analysis revealed that the three architectures had similar porosity and interconnectivity, but having different mean pore sizes as summarized in Table 1, and the pore size distributions are shown in Figure 8. ANOVA tests were carried out to investigate if there are any statistically significant differences in each structural feature between the different architectures. The mean pore size was statistically significantly different for each architecture: $F(2, 6) = 218.7$, $p < 0.0005$, $\Omega^2 = 0.98$ and partial $\eta^2 = 0.99$. Based on the Cohen's effect size benchmarks [41,42], the η^2 values of 0.01, 0.06 and 0.14 correspond to small, medium and large effect size classes, respectively. The pairwise differences were investigated with the Tukey's posthoc analysis. There was a statistically significant difference of 165.1 (95% CI: 40.1, 190.1) between architectures A and B (mean [M] = 555.3, standard error [SE] = 9.0) and a difference of 45.5 (95% CI: 20.5, 70.5) in mean pore size between architecture A (M = 600.8, SE = 3.8) and architecture C (M = 435.7, SE = 2.2). When architectures B and C were compared, there was a statistically significant difference of 119.6 (95% CI: 94,6, 144.6; $p < 0.0005$). The architectures were not statistically significantly different regarding the porosity $F(2, 6) = 0.892$; $p = 0.458$, and interconnectivity. $F(2, 6) = 1.034$; $p = 0.411$.

The null hypothesis in the ANOVA tests was that the means of the samples with architectures A–C are equal for a structural property; and the alternative hypothesis was that at least the mean of one architecture is different. For the mean pore size, the null hypothesis was rejected, and the alternative hypothesis was accepted since the means of the groups were statistically significantly different; and the null hypothesis cannot be rejected for porosity and interconnectivity.

The entire data were checked for the presence of outliers, normal distribution and homogeneity of variances to ensure statistically valid results by confirming the assumptions that underlie the ANOVA tests were met. There were no outliers as assessed by inspection of a box plot for values of >1.5 box lengths from the edge of the box. The data were normally distributed as determined by Shapiro–Wilk's test ($p > 0.05$). There was homogeneity of variances confirmed by Levene's test for equality of variances ($p = 0.093$ for mean pore size, $p = 0.716$ for porosity, $p = 0.241$ for interconnectivity).

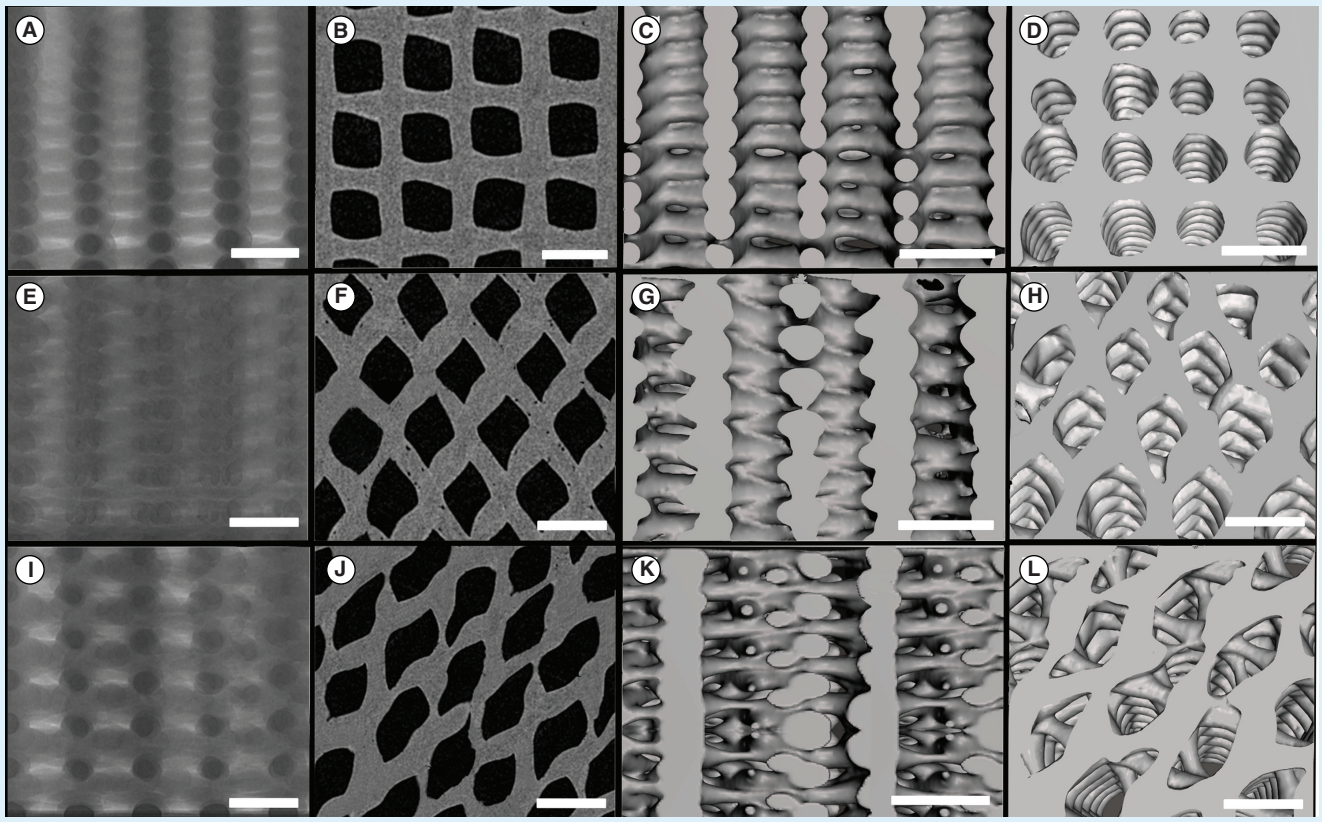

Figure 7. The μ-CT images of the 3D printed samples with the three different internal architectures. (Top row: A–D) A (0°/90° strand structure), **(middle row: E–H)**, B (0°/60°/120° strand structure) and **(bottom row: I–L)** C (0°/45°/90°/135° strand structure): the x-ray images **(A, E and I)**, the 2D reconstructed microcomputed tomography images **(B, F and J)**, the 3D reconstructed images showing the structures from side **(C, G and K)** and top **(D, H and L)** (scale bars: 1 mm).

The size of the pores is one of the important features of a scaffold since it influences the cell attachment, growth and matrix production [43–46]. In the present study, the architecture of PCL scaffolds B and C, which possess micropores, is more adequate for cell culturing as compared with PCL scaffold A (Figure 8). Rebelo *et al.* [47] reviewed the cellular morphometry and characteristics of IVD. It was reported that the fibroblasts have the diameter of 1–20 μm and the chondrocytes have the size of around 10–30 μm. The convenience of diffusion and migration of cells is related to relatively larger sized pores, while cell adhesion is related to relatively smaller sized pores since the relative surface area is larger [45]. Matsiko *et al.* [48] demonstrated that the microarchitecture of the scaffold has a role in differentiation and matrix synthesis of cells. Among the scaffolds they studies, they reported that the scaffolds with the mean pore size

Table 1. The structural and morphometric properties of the scaffolds with the three distinct internal architectures of A (0°/90° strand structure), B (0°/60°/120° strand structure) and C (0°/45°/90°/135° strand structure).

Internal architecture	A	B	C
Porosity (%) M(SE)	45.8 (0.9)	45.8(1.3)	44.1 (1.0)
Mean pore size (μm) M(SE)	600.8 (3.8)	555.3 (9.0)	435.7 (2.2)
Interconnectivity (%) M(SE)	99.2 (0.1)	99.0 (0.1)	99.1 (0.1)

M: Mean; SE: Standard error.

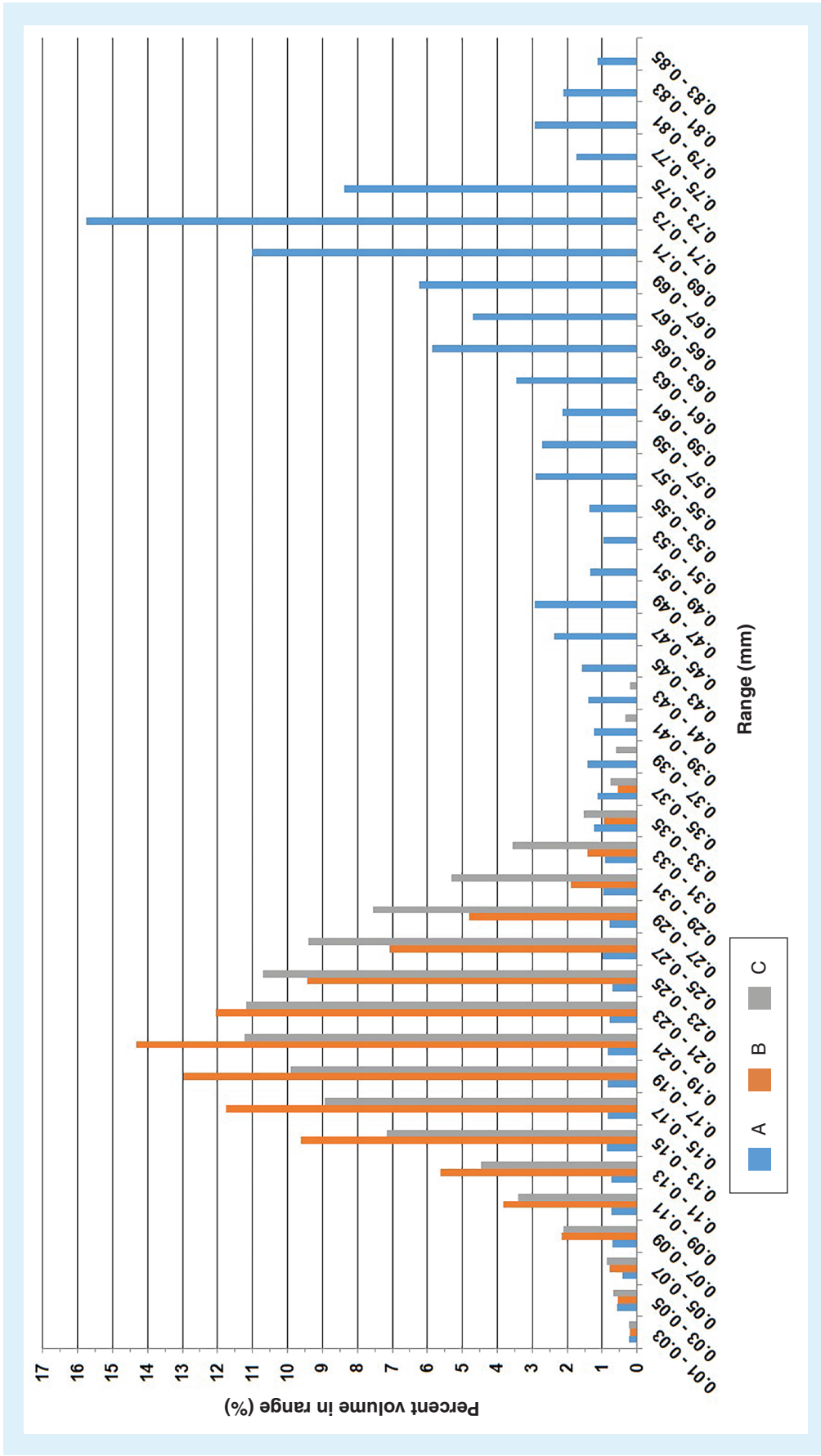

Figure 8. The pore size distribution of the samples with the three distinct internal architectures. (A) (0°/90° strand structure), **(B)** (0°/60°/120° strand structure) and **(C)** (0°/45°/90°/135° strand structure).

of 300 µm provided higher cell growth, like matrix production compared with the scaffolds with the smaller mean pore size that are 94 and 130 µm [48]. Zhang *et al.* [49] 3D-printed PCL scaffolds with three different mean pore sizes, 215, 320 and 515 µm. The authors reported that the scaffolds with the mean pore size of 215 µm had relatively higher cell growth and matrix synthesis *in vitro*, and better performance compared with others *in vivo* [49].

In brief, future studies should further investigate the effect of the scaffold microstructure on the biological and biomechanical performance in a broader manner, that is, considering not only the mean pore size but also the mean porosity and mean wall thickness of the scaffolds.

Conclusion

This study showed a semiautomatic methodology of a geometry reconstruction pipeline from volumetric medical image data to 3D meshes of patient-specific IVD model. The obtained 3D model was 3D printed into scaffolds with different internal architectures. The present work steers us toward the patient-specific IVD TE concept as demonstrated in a way of manufacturing patient-specific scaffolds using the 3D model obtained from the patient's MRI. Furthermore, the obtained patient-specific model could aid in the improvement of clinical and surgical planning before treatment.

Financial & competing interests disclosure

The authors would like to acknowledge the financial support provided by the Portuguese Foundation for Science and Technology (FCT) through the project EPIDisc (UTAP-EXPL/BBB-ECT/0050/2014), funded in the Framework of the 'International Collaboratory for Emerging Technologies, CoLab', UT AustinlPortugal Program. FCT is also acknowledged for the PhD scholarship attributed to IF Cengiz (SFRH/BD/99555/2014) and the financial support provided to J Silva-Correia (SFRH/BPD/100590/2014 and IF/00115/2015). JM Oliveira also thanks the FCT for the funds provided under the program Investigador FCT (IF/00423/2012 and IF/01285/2015). The authors have no other relevant affiliations or financial involvement with any organization or entity with a financial interest in or financial conflict with the subject matter or materials discussed in the manuscript apart from those disclosed.

No writing assistance was utilized in the production of this manuscript.

Ethical conduct of research

The authors state that they have obtained appropriate institutional review board approval or have followed the principles outlined in the Declaration of Helsinki for all human or animal experimental investigations. In addition, for investigations involving human subjects, informed consent has been obtained from the participants involved.

Executive summary

- The clinical need has not been yet completely met to treat intervertebral disc (IVD) problems, and there is a need for regenerative tissue engineering (TE) strategies.
- Scaffolds hold a critical role in IVD TE.
- Given the fact that IVDs differ in size and shape, being patient-specific holds a great importance.
- To show how to produce patient-specific IVD scaffolds/implants, we presented a methodology for producing such 3D-printed scaffolds from human MRI using a semiautomatic 3D segmentation.
- Scaffolds with different internal architectures were produced, and their effect on the microstructure was compared with get preindications on their biological performances with cells.
- Medical imaging combined with the 3D-printing technology enables us to proceed directly to produce patient-specific implants from the chosen biomaterial/s.
- The results bring us a step closer to the development of patient-specific IVD TE scaffold, and the translation into daily clinical approaches is envisioned with future studies.

References

Papers of special note have been highlighted as:
• of interest; •• of considerable interest

1 Shankar H, Scarlett JA, Abram SE. Anatomy and pathophysiology of intervertebral disc disease. *Tech. Reg. Anesth. Pain Manag.* 13(2), 67–75 (2009).

2 Silva-Correia J, Correia SI, Oliveira JM, Reis RL. Tissue engineering strategies applied in the regeneration of the human intervertebral disk. *Biotechnol. Adv.* 31(8), 1514–1531 (2013).

• **Provides the reader a very good overview of the intervertebral disc (IVD) tissue engineering.**

3 Nerurkar NL, Elliott DM, Mauck RL. Mechanical design criteria for intervertebral disc tissue engineering. *J. Biomech.* 43(6), 1017–1030 (2010).

4 Adams MA, Roughley PJ. What is intervertebral disc degeneration, and what causes it? *Spine* 31(18), 2151–2161 (2006).

• **Provides the reader a very good overview of the IVD anatomy, physiology and degeneration.**

5 Adams MA, Dolan P. Intervertebral disc degeneration: evidence for two distinct phenotypes. *J. Anat.* 221(6), 497–506 (2012).

6 Depalma MJ, Ketchum JM, Saullo TR. Multivariable analyses of the relationships between age, gender, and body mass index and the source of chronic low back pain. *Pain Med.* 13(4), 498–506 (2012).

7 Lebow RL, Adogwa O, Parker SL, Sharma A, Cheng J, Mcgirt MJ. Asymptomatic same-site recurrent disc herniation after lumbar discectomy: results of a prospective longitudinal study with 2-year serial imaging. *Spine* 36(25), 2147–2151 (2011).

8 Cowan JA Jr, Dimick JB, Wainess R, Upchurch GR Jr, Chandler WF, La Marca F. Changes in utilization of spinal fusion in the United States. *Neurosurgery* 59(1), 15–20 (2006).

9 Whatley BR, Wen X. Intervertebral disc (IVD): structure, degeneration, repair and regeneration. *Mater. Sci. Eng. C* 32(2), 61–77 (2012).

• **Provides the reader a very good overview of the IVD degeneration and repair.**

10 Barrey C, Perrin G, Champain S. Pedicle-screw-based dynamic systems and degenerative lumbar diseases: biomechanical and clinical experiences of dynamic fusion with isobar TTL. *ISRN Orthop.* 2013, 183702 (2013).

11 Silva-Correia J, Oliveira JM, Caridade SG *et al.* Gellan gum-based hydrogels for intervertebral disc tissue-engineering applications. *J. Tissue Eng. Regen. Med.* 5(6), e97–107 (2011).

12 Silva-Correia J, Miranda-Gonçalves V, Salgado AJ *et al.* Angiogenic potential of gellan-gum-based hydrogels for application in nucleus pulposus regeneration: *in vivo* study. *Tissue Eng. Part A* 18(11–12), 1203–1212 (2012).

13 Pereira D, Silva Correia J, Oliveira JM, Reis R. Hydrogels in acellular and cellular strategies for intervertebral disc regeneration. *J. Tissue Eng. Regen. Med.* 7(2), 85–98 (2013).

•• **Provides the reader a very good overview of the hydrogels for IVD regeneration.**

14 Reitmaier S, Kreja L, Gruchenberg K *et al. In vivo* biofunctional evaluation of hydrogels for disc regeneration. *Eur. Spine J.* 23(1), 19–26 (2014).

15 Silva-Correia J, Gloria A, Oliveira MB *et al.* Rheological and mechanical properties of acellular and cell laden methacrylated gellan gum hydrogels. *J. Biomed. Mater. Res. A* 101(12), 3438–3446 (2013).

16 Mizuno H, Roy AK, Vacanti CA, Kojima K, Ueda M, Bonassar LJ. Tissue-engineered composites of anulus fibrosus and nucleus pulposus for intervertebral disc replacement. *Spine* 29(12), 1290–1297 (2004).

17 Saad L, Spector M. Effects of collagen type on the behavior of adult canine annulus fibrosus cells in collagen–glycosaminoglycan scaffolds. *J. Biomed. Mater. Res. A* 71(2), 233–241 (2004).

18 Shao X, Hunter CJ. Developing an alginate/chitosan hybrid fiber scaffold for annulus fibrosus cells. *J. Biomed. Mater. Res. A* 82(3), 701–710 (2007).

19 Van Uden S, Silva-Correia J, Correlo V, Oliveira J, Reis R. Custom-tailored tissue engineered polycaprolactone scaffolds for total disc replacement. *Biofabrication* 7(1), 015008 (2015).

20 Park SH, Gil ES, Mandal BB *et al.* Annulus fibrosus tissue engineering using lamellar silk scaffolds. *J. Tissue Eng. Regen. Med.* 6(S3), S24–S33 (2012).

21 Park SH, Gil ES, Cho H *et al.* Intervertebral disk tissue engineering using biphasic silk composite scaffolds. *Tissue Eng. Part A* 18(5–6), 447–458 (2011).

22 Cengiz IF, Pitikakis M, Cesario L *et al.* Building the basis for patient-specific meniscal scaffolds: from human knee MRI to fabrication of 3D printed scaffolds. *Bioprinting* 1–2, 1–10 (2016).

•• **Successfully produced patient-specific implants from MRI data.**

23 Radenkovic D, Solouk A, Seifalian A. Personalized development of human organs using 3D printing technology. *Med. Hypotheses* 87, 30–33 (2016).

24 Lertudomphonwanit T, Keorochana G, Kraiwattanapong C, Chanplakorn P, Leelapattana P, Wajanavisit W. Anatomic considerations of intervertebral disc perspective in lumbar posterolateral approach via Kambin's triangle: cadaveric study. *Asian Spine J.* 10(5), 821–827 (2016).

25 Cevidanes LH, Tucker S, Styner M *et al.* Three-dimensional surgical simulation. *Am. J. Orthod. Dentofacial Orthop.* 138(3), 361–371 (2010).

26 Gander T, Essig H, Metzler P *et al.* Patient specific implants (PSI) in reconstruction of orbital floor and wall fractures. *J. Craniomaxillofac. Surg.* 43(1), 126–130 (2015).

27 Kozakiewicz M, Elgalal M, Walkowiak B, Stefanczyk L. Technical concept of patient-specific, ultrahigh molecular weight polyethylene orbital wall implant. *J. Craniomaxillofac. Surg.* 41(4), 282–290 (2013).

28 Pham DL, Xu C, Prince JL. Current methods in medical image segmentation. *Annu. Rev. Biomed. Eng.* 2(1), 315–337 (2000).

29 RheumaSCORE. www.research.softeco.it/rheumascore.aspx (2016).

30 Softeco Sismat S.r.l. www.softeco.it (2016).

31 Parascandolo P, Cesario L, Vosilla L, Viano G. Computer aided diagnosis: state-of-the-art and application to musculoskeletal diseases. In: *3D Multiscale Physiological Human*, Magnenat-Thalmann N, Ratib O, Choi HF (Eds). Springer-Verlag, London, UK, 277–296 (2014).

32 Yushkevich PA, Piven J, Hazlett HC *et al.* User-guided 3D active contour segmentation of anatomical structures: significantly improved efficiency and reliability. *Neuroimage* 31(3), 1116–1128 (2006).

33 3Dslicer. www.slicer.org (2016).

34 Cates JE, Lefohn AE, Whitaker RT. GIST: an interactive, GPU-based level set segmentation tool for 3D medical images. *Med. Image Anal.* 8(3), 217–231 (2004).

35 Analyze. www.analyzedirect.com (2016).

36 Parascandolo P, Cesario L, Vosilla L, Pitikakis M, Viano G. Smart Brush: a real time segmentation tool for 3D medical images. Presented at: *8th International Symposium on Image and Signal Processing and Analysis (ISPA)*, Trieste, Italy, September 4–6, 2013.

• **Successfully showed 3D segmentation on medical images.**

37 Caselles V, Kimmel R, Sapiro G. Geodesic active

contours. Presented at: *Proceedings of the Fifth International Conference on Computer Vision*. Cambridge, MA, USA, June 20–23, 1995.

38 Wong KP. Medical image segmentation: methods and applications in functional imaging. In: *Handbook of Biomedical Image Analysis*. Suri JS, Wilson DL, Laxminarayan S (Eds). Springer-Verlag, London, UK, 111–182 (2005).

39 Cortez S, Claro JCP, Alves J. 3D reconstruction of a spinal motion segment from 2D medical images: objective quantification of the geometric accuracy of the FE mesh generation procedure. Presented at: *IEEE 3rd Portuguese Meeting in Bioengineering (ENBENG)*. Braga, Portugal, February 20–23, 2013.

40 Kimmel R. *Numerical Geometry of Images: Theory, Algorithms, and Applications*. Springer-Verlag, NY, USA (2012).

41 Cohen J. *Statistical Power Analysis for the Behavioral Sciences* (2nd Edition). Lawrence Erlbaum Associates, NJ, USA (1988).

42 Ellis PD. *The Essential Guide to Effect Sizes: Statistical Power, Meta-Analysis, and The Interpretation of Research Results*. Cambridge University Press, Cambridge, UK (2010).

43 Murphy CM, Duffy GP, Schindeler A, O'brien FJ. Effect of collagen–glycosaminoglycan scaffold pore size on matrix mineralization and cellular behavior in different cell types. *J. Biomed. Mater. Res. A* 104(1), 291–304 (2016).

44 Zhang Q, Lu H, Kawazoe N, Chen G. Pore size effect of collagen scaffolds on cartilage regeneration. *Acta Biomater.* 10(5), 2005–2013 (2014).

45 O'brien FJ, Harley B, Yannas IV, Gibson LJ. The effect of pore size on cell adhesion in collagen–GAG scaffolds. *Biomaterials* 26(4), 433–441 (2005).

46 Murphy CM, Haugh MG, O'brien FJ. The effect of mean pore size on cell attachment, proliferation and migration in collagen–glycosaminoglycan scaffolds for bone tissue engineering. *Biomaterials* 31(3), 461–466 (2010).

47 Rebelo MA, Alves TF, De Lima R *et al.* Scaffolds and tissue regeneration: an overview of the functional properties of selected organic tissues. *J. Biomed. Mat. Res. Part B: Applied Biomaterials*. 104 (7) 1483–1494 (2016).

48 Matsiko A, Gleeson JP, O'brien FJ. Scaffold mean pore size influences mesenchymal stem cell chondrogenic differentiation and matrix deposition. *Tissue Eng. Part A* 21(3–4), 486–497 (2014).

49 Zhang ZZ, Jiang D, Ding JX *et al.* Role of scaffold mean pore size in meniscus regeneration. *Acta Biomater.* 43, 314–326 (2016).